Motion of discrete interfaces on the triangular lattice

Giovanni Scilla

Abstract. We study the motion of discrete interfaces driven by ferromagnetic interactions on the two-dimensional triangular lattice by coupling the Almgren, Taylor and Wang minimizing movements approach and a discrete-to-continuum analysis, as introduced by Braides, Gelli and Novaga in the pioneering case of the square lattice. We examine the motion of origin-symmetric convex "Wulff-like" hexagons, i.e. origin-symmetric convex hexagons with sides having the same orientations as those of the hexagonal Wulff shape related to the density of the anisotropic perimeter Γ-limit of the ferromagnetic energies as the lattice spacing vanishes. We compare the resulting limit motion with the corresponding evolution by crystalline curvature with natural mobility.

Mathematics Subject Classification (2010). 35B27, 74Q10, 53C44, 49M25.

Keywords. discrete systems, minimizing movements, wulff shape, motion by curvature, crystalline curvature, triangular lattice, natural mobility.

1. Introduction

This paper is concerned with the variational motion of discrete interfaces arising from nearest-neighbours ferromagnetic-type interactions on the 2D triangular lattice. Our analysis aims to do a first step in the challenging and still largely open problem of characterizing the evolution of discrete interfacial energies driving more general atomistic systems in presence of dissipation. The choice of the triangular lattice in dimension two seems to be natural, since it is the local equilibrium state for some interatomic potentials (see, e.g., [41]), and the adequate framework for some discrete problems in crystallization (see, e.g., [6, 28] and the references therein); discrete models in fracture mechanics [15, 16], elasticity [24], magnetism [7], topological defects [29] and some physical models for two-dimensional fluids as the Bell-Lavis model [9, 10]. Since crystalline perimeter energies can be approximated by lattice energies via Γ-convergence (see, e.g., [1, 19]) and arise in the study of evolutions by anisotropic curvature [3, 25, 39, 40, 36, 37, 38], the problem

we address is also motivated by the analysis of the discreteness effects on such motions and their numerical approximation [26, 27]. Moreover, geometric evolutions with underlying lattice can be interpreted as a simple version of motion of fronts or interfaces propagating in heterogeneous environments (see, e.g., [8, 30]).

The Almgren, Taylor and Wang (ATW) approach to curvature-driven motions. The analysis will be carried over by using the minimizing-movements scheme of Almgren, Taylor and Wang [3] for geometric evolutions driven by crystalline curvature. This consists in introducing a time scale τ, an initial set E_0^τ and iteratively defining a sequence of sets $\{E_k^\tau\}_{k\geq 1}$ as minimizers of

$$\min\left\{\int_{\partial E}\|\nu\|_1 \mathrm{d}\mathcal{H}^1 + \frac{1}{\tau}\int_{E\triangle E_{k-1}^\tau}\mathrm{dist}(x,\partial E_{k-1}^\tau)\,\mathrm{d}x\right\}, \tag{1.1}$$

among the sets of finite perimeter, where the first term is the *crystalline perimeter* of E and $\int_{E\triangle F}\mathrm{dist}(x,\partial F)\,\mathrm{d}x$ accounts for the L^2-distance between the boundaries of sets E, F. In (1.1), ∂E is the boundary of E, $\|\cdot\|_1$ denotes the ℓ^1-norm, $\mathcal{H}^1$ is the 1-dimensional Hausdorff measure and $E\triangle F$ stands for the symmetric difference between E and F. Once the time-discrete sequence $\{E_k^\tau\}_{k\geq 1}$ has been constructed, one computes a time-continuous limit (the *flat flow*) $E(t)$ of the piecewise constant interpolations $E^\tau(t) := E^\tau_{\lfloor t/\tau\rfloor}$ as $\tau\to 0$, which defines the motion by *crystalline curvature* [2]

$$V(t) = \kappa(t), \tag{1.2}$$

as introduced independently by J. Taylor [37] and Angenent-Gurtin [5]. According to (1.2), each side of a set with polygonal boundary moves inward along its normal direction with a velocity V coinciding with its crystalline curvature κ, that is proportional to the inverse of its length. In general, when dealing with an *anisotropic perimeter* of the form

$$\Phi(E) = \int_{\partial E}\varphi(\nu)\,\mathrm{d}\mathcal{H}^1,$$

for φ any norm on $\mathbb{R}^2$, existence and uniqueness for the motion by crystalline curvature are simply proved for the class of "good" polygonal curves (see [37, Prop. 2.1.1]). That is the case, for instance, if the initial set is a convex *Wulff-like* set; i.e., it has a polygonal boundary whose sides have the same exterior unit normal vectors and form the same angles as those of the *Wulff shape* $\mathcal{W}_\varphi$ of the density φ, where

$$\mathcal{W}_\varphi := \Big\{x\in\mathbb{R}^2 \,|\, \langle x,\nu\rangle \leq \varphi(\nu) \quad \text{for every } \nu \text{ such that } |\nu| = 1\Big\},$$

$\langle\cdot,\cdot\rangle$ being the scalar product on $\mathbb{R}^2$. It is well known that $\mathcal{W}_\varphi$ is a centrally symmetric convex polygon and coincides with the unit ball $\{\varphi^\circ\leq 1\}$ of the dual norm φ° (see, e.g., [32]).

The (ATW) scheme implemented for energies

$$\int_{\partial E}\varphi(\nu)\,\mathrm{d}\mathcal{H}^1 + \frac{1}{\tau}\int_{E\triangle E_{k-1}^\tau}\inf_{y\in\partial E_{k-1}^\tau}\varphi^\circ(x-y)\,\mathrm{d}x \tag{1.3}$$

gives, in the limit as $\tau \to 0$, the motion by crystalline curvature with *natural mobility*

$$V(t) = M(n)\kappa(t), \tag{1.4}$$

where the mobility $M = \varphi$ is a function of the unit normal vector n of the side (see, e.g., [36, 39, 40, 38, 25]). More precisely, the evolution is governed by equations

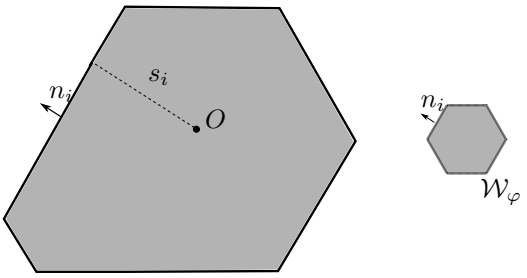

Figure 1. The function $s_i(t)$ is the distance from a fixed origin O of a side with length $L_i(t)$ and normal vector n_i.

$$\dot{s}_i(t) = -\varphi(n_i)\frac{\Lambda(n_i)}{L_i(t)}, \quad i = 1, \dots, m, \tag{1.5}$$

where m is the number of sides of the initial set, s_i is the distance from a fixed origin O of a side with normal vector n_i and length L_i, and $\Lambda(n_i)$ is the length of the side of the Wulff-shape having n_i as normal vector (see Fig. 1 for an example with φ an hexagonal norm).

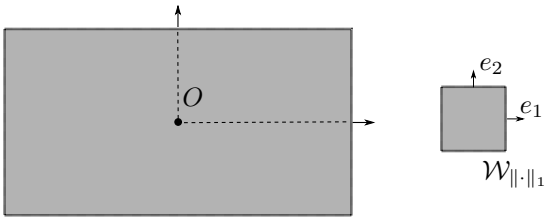

Figure 2. In the case $\varphi = \|\cdot\|_1$, a convex 'Wulff-like' set is a coordinate rectangle.

For instance, if $\varphi(\nu) = \|\nu\|_1$ (see Fig. 2) then its Wulff shape is the coordinate square $\mathcal{W}_{\|\cdot\|_1} = \{\|x\|_\infty \le 1\}$, so $n_i \in \{\pm e_1, \pm e_2\}$, $i = 1, \dots, 4$, $\varphi(n_i) \equiv 1$ and $\Lambda(n_i) \equiv 2$. Thus, in the case of initial datum a coordinate rectangle (a convex 'Wulff-like' set), the evolution by crystalline curvature (1.5) is a rectangle with the same centre and sides of lengths $L_1(t), L_2(t)$

solution to the system of ordinary differential equations

$$\begin{cases} \dot{L}_1(t) = -\dfrac{4}{L_2(t)} \\ \\ \dot{L}_2(t) = -\dfrac{4}{L_1(t)}, \quad t \in [0,T]. \end{cases}$$

Motion of discrete interfaces: the state of the art. In a pioneering paper by Braides, Gelli and Novaga [17] the (ATW) approach (1.1) has been coupled with a homogenization procedure via Γ-convergence. In this case the perimeters and the distances depend on a small parameter $\varepsilon > 0$ (the space scale), and consequently, after introducing a time scale τ, $E_0^{\tau,\varepsilon}$ such that $\mathrm{d}_{\mathcal{H}}(E_0^{\tau,\varepsilon}, E_0) \to 0$ for some regular limit set E_0 ($\mathrm{d}_{\mathcal{H}}$ being the Hausdorff distance between sets), the time-discrete motions are the sets $E_k^{\tau,\varepsilon}$ defined iteratively by

$$E_k^{\tau,\varepsilon} \in \operatorname{argmin}\Big\{ P_\varepsilon(E) + \frac{1}{\tau}\int_{E \triangle E_{k-1}^{\tau,\varepsilon}} d_\infty^\varepsilon(x, \partial E_{k-1}^{\tau,\varepsilon})\,\mathrm{d}x \Big\}, \quad k \geq 1, \tag{1.6}$$

where the minimization is over finite unions of squares with side-length ε. The energies P_ε are *discrete ferromagnetic energies* (see Remark 2.1 for a physical interpretation), defined on subsets of the square lattice $E \subset \varepsilon\mathbb{Z}^2$, of the form

$$P_\varepsilon(E) = \frac{1}{2}\,\varepsilon\,\#\Big\{(i,j) \in \varepsilon\mathbb{Z}^2 \times \varepsilon\mathbb{Z}^2 : i \in E, j \notin E,\ |i-j| = \varepsilon\Big\}, \tag{1.7}$$

each couple (i,j) being accounted twice. After a piecewise constant identification of E with a subset of $\mathbb{R}^2$, the P_ε can be interpreted as the perimeter of E. The continuum (Γ-)limit of these energies as $\varepsilon \to 0$ is the crystalline perimeter

$$P(E) = \int_{\partial E} \|\nu\|_1 \mathrm{d}\mathcal{H}^1, \tag{1.8}$$

as proven by Alicandro, Braides and Cicalese [1]. The distance d_∞^ε in (1.6) is a suitable discretization of the L^∞-distance from the boundary of the previous set.

The time-continuous limit $E(t)$ of $E_{\lfloor t/\tau \rfloor}^{\tau,\varepsilon}$ defined in (1.6) then may depend how mutually ε and τ tend to 0 (Braides [14, Theorem 8.1]). In particular, if $\tau/\varepsilon \to 0$ the limit motion will be *pinned*; i.e., $E(t) \equiv E_0$ (in a sense, we can pass to the limit in τ first, and then apply the (ATW) approach). On the contrary, if $\tau/\varepsilon \to +\infty$ then the limit $E(t)$ will be the crystalline evolution related to the limit P defined in (1.8) (again, in a sense, in this case we can pass to the limit in ε first). The relevant regime which gives the most information about all the limit evolutions is when $\tau/\varepsilon \to \gamma \in (0, +\infty)$. Within this scaling, every evolution with initial datum a coordinate rectangle is still a coordinate rectangle and, in case of uniqueness, the side-lengths $L_1(t), L_2(t)$ of

this rectangle solve a system of "degenerate" ordinary differential equations

$$\begin{cases} \dot{L}_1(t) = -\dfrac{2}{\gamma}\left\lfloor \dfrac{2\gamma}{L_2(t)} \right\rfloor \\ \\ \dot{L}_2(t) = -\dfrac{2}{\gamma}\left\lfloor \dfrac{2\gamma}{L_1(t)} \right\rfloor, \end{cases} \tag{1.9}$$

for almost every t until the extinction time. We note that the discontinuous form of the right-hand sides highlights that the microscopic motion is obtained by overcoming some energy barriers in a 'quantized' manner. As a consequence, large rectangles stay pinned: if both initial side-lengths are above the *pinning threshold* $\widetilde{L} = 2\gamma$ then the right-hand sides in (1.9) are zero and the motion is pinned.

These unexpected features of the limit motions led many authors to investigate the sensibility of such evolutions to microstructure, showing that they may be affected of microscopic properties not detected in the limit description. We mention [20] and [35] in case of 'high-contrast' and 'low-contrast' periodic media, respectively, where the dependence of the limit velocity on the curvature is described by a homogenized formula quite different with respect to that found in [17]. Indeed, the periodic microstructure may act as a selection criterion for the discrete minimizers, thus producing acceleration/deceleration effects on the limit velocity with respect to the homogeneous case [17]. A random counterpart of the low-contrast setting has been provided in [34]. Recently, in [13] the case of antiferromagnetic energies, in particular anti-phase boundaries between striped patterns, has been investigated, showing the appearance of some non-local curvature dependence velocity law reflecting the creation of some defect structure on the interface at the microscopic level. The paper [23], instead, deals with the motion of discrete interfaces through *mushy layers* in high-contrast spin systems and the consequent creation of bulk microstructure. A first approach to *time-reversed* motions, in any dimension, can be found in [21], where a suitably scaled discrete version of the (ATW) scheme, with a negative perimeter term and the ℓ^∞-dissipation, has been used. Therein, the corresponding discrete minimizers have a "checkerboard" structure, and the limit evolution is a family of cubes nucleating from a point and expanding with constant velocity. A more general result in this direction, still in dimension two and for dissipations associated to any absolute norm (and also some strongly anisotropic norm), will be the content of a forthcoming paper [22]. We mention also [18, 31] for effective crystalline evolutions resulting from microstructures modeled through periodic forcing terms.

Our result. However, there is a lack in literature of a discrete-to-continuum analysis as in [17] on a different lattice than $\mathbb{Z}^2$ and for a more general dissipation term than the ℓ^∞-norm. This motivates our contribution, which addresses the problem in the simple case of lattice energies as in (1.7) labeled by the nodes of the *triangular lattice* $\mathbb{T}$. The variational continuous limit of

these energies as $\varepsilon \to 0$ is an anisotropic perimeter

$$P(E) = \int_{\partial E} \varphi_{hex}(\nu) \mathrm{d}\mathcal{H}^1,$$

whose density φ_{hex} is a norm with hexagonal symmetries (see Proposition A.4 in the Appendix A), and the corresponding Wulff shape $\mathcal{W}_{hex}$ is a regular hexagon.

In the discrete formulation of the (ATW) scheme (1.3), we restrict our analysis to initial limit sets that are convex origin-symmetric *Wulff-like hexagons* (see Definition 3.1 for a precise definition). These sets, whose geometry is compatible with the level sets of the dissipation φ°_{hex}, can be seen as the equivalent of coordinate rectangles in [17], and we believe that the investigation of the motion of more general sets - that goes beyond the scope of this paper - may be helped by the study of these ones.

In the case of initial datum a convex origin-symmetric Wulff-like hexagon, with Proposition 3.4 we prove that the resulting evolution is a set of the same type. Indeed, each connected component of the evolution is a convex Wulff-like hexagon, since a Wulff-like convexification provides a competitor with less energy in the minimization problem. Then, an argument based on suitable translations towards the origin shows that the evolution is actually connected. In addition, it contains the origin and, in fact, it is origin-symmetric as shown by the explicit computation of the minimizer. Furthermore, the underlying lattice forces the velocities to be quantized and possibly not uniquely defined for certain values of the curvature. Indeed, each side of length $L_i(t)$ with exterior unit normal vector n_i moves inward in the direction n_i, and its distance $s_i(t)$ from the origin reduces with velocity $v_i(t)$ satisfying the inclusions

$$v_i(t) \begin{cases} = \dfrac{\sqrt{3}}{2\gamma} \left\lfloor \dfrac{\alpha_{hex}\gamma}{L_i(t)} \right\rfloor, & \text{if } \dfrac{\alpha_{hex}\gamma}{L_i(t)} \notin \mathbb{N} \\ \in \dfrac{\sqrt{3}}{2\gamma} \left[\left(\dfrac{\alpha_{hex}\gamma}{L_i(t)} - 1 \right), \dfrac{\alpha_{hex}\gamma}{L_i(t)} \right], & \text{if } \dfrac{\alpha_{hex}\gamma}{L_i(t)} \in \mathbb{N}, \end{cases}$$

where the "mobility factor" α_{hex} is equal to $\frac{16}{9}$.

As a consequence, in the case of a unique evolution, the side-lengths $L_i(t)$ solve the system of degenerate ordinary differential equations

$$\dot{L}_i(t) = \frac{1}{\gamma} \left\lfloor \frac{\alpha_{hex}\gamma}{L_i(t)} \right\rfloor - \frac{1}{\gamma} \left(\left\lfloor \frac{\alpha_{hex}\gamma}{L_{i-1}(t)} \right\rfloor + \left\lfloor \frac{\alpha_{hex}\gamma}{L_{i+1}(t)} \right\rfloor \right), \tag{1.10}$$

for every $i = 1, \dots, 6$, for almost every t, where the labelling of the sides is intended to be modulo 6. Clearly, by (1.10), if all the side lengths L_i^0 of the initial limit set are larger than $\alpha_{hex}\gamma$, then none of the sides can move and the motion coincides identically with the initial set. The pinning threshold $\alpha_{hex}\gamma$ is computed by imposing that the minimal inward displacement of a side along its normal direction is not energetically convenient (see Section 3.1). We point out that also some *partial pinning* phenomena may occur; that is,

a side stays pinned until it shortens sufficiently due to the motion of the adjacent sides (see Section 3.3 for an example).

Eventually, when the initial datum is a (sufficiently small) Wulff shape, the function $s_i(t) \equiv s(t)$ is independent of the side and coincides with the apothem of the shrinking hexagon. In this case we have a self-similar evolution and the system (1.10) reduces to a single equation approximating the corresponding crystalline evolution with natural mobility.

As a final remark, we mention that the knowledge of the evolution of the Wulff shape is a key tool when investigating the motion of more general (possibly non-convex and non-symmetric) sets, both in the continuous (see, e.g., [2, Sections 5.1-5.2]) and in the discrete setting (cf. [17, Theorem 3]). In particular, it allows to deduce an upper bound on the Hausdorff distance between the boundaries of successive minimizers of the (ATW) scheme and then, coupled with the isoperimetric inequality, to prove the connectedness of each minimizer.

Plan of the paper. The paper is organized as follows. In Section 2 we fix notation and introduce the energies we will consider on the triangular lattice. We then formulate the discrete analogous of the Almgren, Taylor and Wang scheme (1.3), according to [17]. Section 3 contains the proof of the convergence of the discrete scheme in the case of an origin-symmetric convex Wulff-like initial set. In Section 3.1 we compute the pinning threshold and the description of the limit motion is contained in Section 3.2. In Section 3.4 we also compare it with the corresponding crystalline evolution. Eventually, the Appendix A contains the proof of the Γ-convergence result for the ferromagnetic energies on the triangular lattice, together with the necessary notation and preliminary results on the involved function spaces and some basic facts about the hexagonal norm we use throughout the paper.

2. Basic notation and setting of the problem

The symbol $|\cdot|$ denotes both the absolute value and Euclidean norm. If $x = (x^1, x^2) \in \mathbb{R}^2$ we set $\|x\|_1 = |x^1| + |x^2|$, $\|x\|_\infty = \max\{|x^1|, |x^2|\}$ and the usual scalar product in $\mathbb{R}^2$ will be denoted by $\langle \cdot, \cdot \rangle$. If A is a Lebesgue-measurable set we indicate by $\mathcal{L}^2(A)$ its two-dimensional Lebesgue measure. The symmetric difference between two sets A and B in $\mathbb{R}^2$ is denoted by $A \triangle B$, their *Hausdorff distance* is defined by

$$\mathrm{d}_{\mathcal{H}}(A, B) = \max\left\{ \sup_{a \in A} \mathrm{dist}(a, B), \sup_{b \in B} \mathrm{dist}(b, A) \right\},$$

where $\mathrm{dist}(x, E)$ is the distance of the point x to the set E defined, as usual, by $\mathrm{dist}(x, E) = \inf_{y \in E} |x - y|$. We say that a sequence of sets $\{E_\varepsilon\}$ converges to E in the Hausdorff sense as $\varepsilon \to 0$ if and only if $\mathrm{d}_{\mathcal{H}}(E_\varepsilon, E) \to 0$ and E is closed.

If E is a set of finite perimeter then $\partial^* E$ is its reduced boundary (see, for example [11]) and the 1-dimensional Hausdorff measure of $\partial^* E$ is denoted

by $\mathcal{H}^1(\partial^* E)$. The measure-theoretical inner normal to E at a point x in $\partial^* E$ is denoted by $\nu = \nu_E(x)$.

If $e = (e^1, e^2)$ is a vector, then we denote by $e^\perp$ the anticlockwise rotation of $\pi/2$ of e; that is, $e^\perp = (-e^2, e^1)$. If $\{a_i\}, i = 1, \dots, N$ is a finite set of vectors, then $\mathrm{conv}(a_1, a_2, \dots, a_N)$ is the *convex hull* of vectors $\{a_i\}$.

2.1. Ferromagnetic energies on triangular lattice

We consider the *triangular lattice* $\mathbb{T} = \mathrm{Span}(\eta_1, \eta_2; \mathbb{Z}^2)$, where $\eta_1 = (1, 0)$, $\eta_2 = (1/2, \sqrt{3}/2)$ and $\mathrm{Span}(\eta_1, \eta_2; \mathbb{Z}^2)$ is the set of all linear combinations of η_1, η_2 with coefficients in $\mathbb{Z}^2$ (see Fig. 3). We also define $\eta_3 := \eta_1 - \eta_2$,

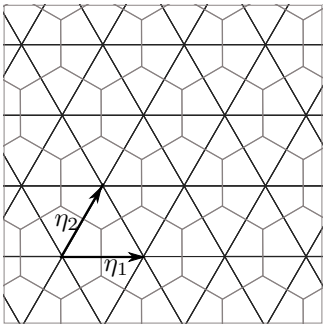

Figure 3. Triangular lattice and its dual (hexagonal) lattice.

$\mathcal{S} := \{\pm\eta_1, \pm\eta_2, \pm\eta_3\}$ the set of the *unitary vectors* in the lattice $\mathbb{T}$ and $\mathcal{R} := \{\eta^\perp : \eta \in \mathcal{S}\}$ the set of *coordinate directions*. With fixed $\varepsilon > 0$, we introduce interfacial energies defined on subsets $\mathcal{I} \subset \varepsilon\mathbb{T}$ as

$$P_\varepsilon(\mathcal{I}) = \frac{\sqrt{3}}{3}\left(\frac{1}{2}\varepsilon \,\#\Big\{(i,j) \in \varepsilon\mathbb{T} \times \varepsilon\mathbb{T} : i \in \mathcal{I}, j \notin \mathcal{I},\ |i-j| = \varepsilon\Big\}\right), \quad (2.1)$$

where each couple (i, j) is accounted twice.

To study the continuous limit as $\varepsilon \to 0$ of these energies it is customary to identify each subset of $\varepsilon\mathbb{T}$ with a measurable subset of $\mathbb{R}^2$, in such a way that equi-boundedness of the energies implies pre-compactness of such sets in the sense of sets of finite perimeter. This identification is as follows: we denote by H the cell of the dual lattice of $\mathbb{T}$ (see Fig 3); that is, the closed regular hexagon of center 0 and side-length $\sqrt{3}/3$ defined by $H = \frac{\sqrt{3}}{3}\mathrm{conv}(\mathcal{R})$. For every $i \in \varepsilon\mathbb{T}$, we denote by $H_\varepsilon(i) = i + \varepsilon H$ the closed regular hexagon with side-length $\frac{\sqrt{3}}{3}\varepsilon$ and centered in i. We refer to each side of $H_\varepsilon(i)$ as a *cell side*. To a set of indices $\mathcal{I} \subset \varepsilon\mathbb{T}$ we associate the set

$$E_{\mathcal{I}} = \bigcup_{i \in \mathcal{I}} H_\varepsilon(i) \subset \mathbb{R}^2.$$

The space of *admissible sets* related to indices in the two-dimensional triangular lattice is then defined by

$$\mathcal{D}_\varepsilon := \Big\{E \subseteq \mathbb{R}^2 : \quad E = E_{\mathcal{I}} \text{ for some } \mathcal{I} \subseteq \varepsilon\mathbb{T}\Big\}, \quad (2.2)$$

and for any $E = E_{\mathcal{I}} \in \mathcal{D}_\varepsilon$ we denote, with abuse of notation,

$$P_\varepsilon(E) = P_\varepsilon(\mathcal{I}) = \mathcal{H}^1(\partial E). \tag{2.3}$$

Remark 2.1. In order to justify the name of *ferromagnetic energies*, we remark that the P_ε as in (2.1) can be viewed as lattice energies; that is, depending on a discrete variable $u = \{u(i)\}$ indexed by the nodes i of $\varepsilon\mathbb{T}$, of the form

$$P_\varepsilon(u) = \frac{\sqrt{3}}{3} \times \frac{1}{4} \sum_{|i-j|=\varepsilon} \varepsilon(u(i) - u(j))^2,$$

where $u(i)$ takes only the two values +1 and -1 (*ferromagnetic energy for Ising spin system*). After identifying u with the set E obtained as the union of all the cells $H_\varepsilon(i)$ such that $u(i) = 1$, the energy P_ε can be equivalently rewritten as a perimeter functional as in (2.3), and hence can be interpreted as a *discrete interfacial energy*.

In [1] it is shown that the Γ-limit's domain of energies P_ε is the family of sets of finite perimeter and its general form is

$$\Phi(E) = \int_{\partial^* E} \varphi(\nu) \mathrm{d}\mathcal{H}^1,$$

where φ is a convex, positively homogeneous of degree one function reflecting the symmetries of the underlying lattice.

We state the Γ-convergence result for energies (2.1), noting that the argument may be deduced from a more general analysis developed for vector-valued lattice energies of Lennard-Jones type [15, Proposition 4.6]. For the interested readers's convenience, we provide a direct proof of Theorem 2.2 with Proposition A.4 in the Appendix.

Theorem 2.2 (Γ-convergence of perimeter energies). *The energies P_ε defined by*

$$P_\varepsilon(E) = \begin{cases} P_\varepsilon(\mathcal{I}), & \text{if } E = E_{\mathcal{I}} \in \mathcal{D}_\varepsilon \\ +\infty, & \text{otherwise} \end{cases}$$

Γ-converge, as $\varepsilon \to 0$, with respect to the L^1-topology to the anisotropic perimeter functional

$$P(E) = \int_{\partial^* E} \varphi_{hex}(\nu)\, \mathrm{d}\mathcal{H}^1, \tag{2.4}$$

whose density φ_{hex} is defined as

$$\varphi_{hex}(\nu) := \frac{2}{3} \sum_{k=1}^{3} |\langle \nu, \eta_k \rangle|. \tag{2.5}$$

2.2. The dissipation term and the minimization scheme

The choice of the dissipation term in the Almgren, Taylor and Wang scheme affects the mobility of the limit interface (see, e.g., [36, Section 1] for a discussion). For instance, considering there the distance induced by the dual norm of the density of the perimeter term as in (1.3), in the limit as $\tau \to 0$

one retrieves the motion by crystalline curvature with natural mobility, governed by equations (1.5). Although this situation is not very general, as a fact of interest in this case the evolution of the Wulff shape is explicit and self-similar (see, e.g., [25]). Another motivation, purely practical, is that the level sets of the resulting distance have the symmetries of the Wulff shape, thus simplifying many computations.

Therefore, in order to define the dissipation term in the (ATW) scheme, we first notice that by virtue of Lemma A.1(ii), the dual norm φ°_{hex} of φ_{hex} is given by

$$\varphi^\circ_{hex}(x) = \frac{\sqrt{3}}{2} \max_{k=1,2,3} |\langle x, \eta_k^\perp \rangle| \,. \tag{2.6}$$

Moreover, (2.6) complies with $\varphi^\circ_{hex}(\mathbb{T}\backslash\{0\}) = \frac{3}{4}\mathbb{N}$, since if $x \in \mathbb{T}\backslash\{0\}$ and $x = n\eta_1 + m\eta_2$ for some $n, m \in \mathbb{Z}$, then $\varphi^\circ_{hex}(x) = \frac{3}{4}\max\{|n|, |m|, |m+n|\}$.

We define a notion of *discrete distance* d^ε induced by φ°_{hex} as

(1) $d^\varepsilon(H_\varepsilon(i), H_\varepsilon(j)) = \varphi^\circ_{hex}(i-j)$, for every $i, j \in \varepsilon\mathbb{T}$;
(2) $d^\varepsilon(E, F) = \inf\{d^\varepsilon(H_\varepsilon(i), H_\varepsilon(j)) : \ H_\varepsilon(i) \in E, \ H_\varepsilon(j) \in F\}$, for every E, $F \in \mathcal{D}_\varepsilon$.

Moreover, for every $x \in E$, we set

$$d^\varepsilon(x, \partial F) := \begin{cases} \inf\{d^\varepsilon(H_\varepsilon(i), H_\varepsilon(j)) : \ x \in H_\varepsilon(i), \ H_\varepsilon(j) \in F\}\,, & \text{if } x \notin F\,, \\ \inf\{d^\varepsilon(H_\varepsilon(i), H_\varepsilon(j)) : \ x \in H_\varepsilon(i), \ H_\varepsilon(j) \notin F\}\,, & \text{if } x \in F\,. \end{cases}$$

Now, we are in position to introduce an analogous time-discrete minimization scheme as in [17]. Specifically, we fix a time step $\tau > 0$ and define a time-discrete motion obtained by successive minimizations of the energy $\mathcal{F}_{\tau,\varepsilon} : \mathcal{D}_\varepsilon \times \mathcal{D}_\varepsilon \to \mathbb{R}$ given by

$$\begin{aligned} \mathcal{F}_{\tau,\varepsilon}(E, F) &= P_\varepsilon(E) + \frac{1}{\tau}\int_{E\triangle F} d^\varepsilon(x, \partial F)\,\mathrm{d}x \\ &= P_\varepsilon(E) + \frac{\sqrt{3}}{2}\frac{\varepsilon^2}{\tau}\left(\sum_{H_\varepsilon(i)\in E\backslash F} d^\varepsilon(H_\varepsilon(i), F) + \sum_{H_\varepsilon(i)\in F\backslash E} d^\varepsilon(H_\varepsilon(i), \mathbb{R}^2\backslash F)\right), \end{aligned} \tag{2.7}$$

where $\frac{\sqrt{3}}{2}\varepsilon^2$ is the area of the hexagonal cell. More precisely, given an initial set $E_0^{\tau,\varepsilon} \in \mathcal{D}_\varepsilon$ approximating, as $\varepsilon, \tau \to 0$ in the Hausdorff sense, a sufficiently regular set E_0, we define recursively a sequence $E_k^{\tau,\varepsilon}$ in $\mathcal{D}_\varepsilon$ by requiring that $E_{k+1}^{\varepsilon,\tau}$ is a minimizer of the functional $\mathcal{F}_{\tau,\varepsilon}(\cdot, E_k^{\tau,\varepsilon})$, for every $k \geq 0$. Then, setting

$$E^{\tau,\varepsilon}(t) = E^{\tau,\varepsilon}_{\lfloor t/\tau \rfloor}, \tag{2.8}$$

for every $t \geq 0$, we are interested in characterizing the motion described by any converging subsequence of $E^{\tau,\varepsilon}(t)$ as $\varepsilon, \tau \to 0$.

As remarked in the Introduction, the interaction between the two discretization parameters, in time and space, plays a crucial role in such a limiting process. More precisely, the limit motion depends strongly on their

relative decrease rate to 0. If $\tau/\varepsilon \to +\infty$, then we may first let $\varepsilon \to 0$, so that $P_\varepsilon(E)$ can be directly replaced by the limit anisotropic perimeter $P(E)$ defined in (2.4) and $\frac{1}{\tau}\int_{E\triangle F} d^\varepsilon(x,\partial F)\,\mathrm{d}x$ by

$$\frac{1}{\tau}\int_{E\triangle F} \inf_{y\in\partial F} \varphi^\circ_{hex}(x-y)\,\mathrm{d}x.$$

As a consequence, the approximated flat motions tend to the solution of the time-continuous ones studied in [2, 37] with natural mobility function $M = \varphi_{hex}$.

On the other hand, if $\tau/\varepsilon \to 0$ then there is no motion ('pinning'), since $E_k^{\tau,\varepsilon} \equiv E_0^{\tau,\varepsilon}$ and the limit evolution is the constant state E_0. Indeed, for any $F \neq E_0^{\tau,\varepsilon}$ and for τ small enough we have

$$\frac{1}{\tau}\int_{E_0^{\tau,\varepsilon}\triangle F} d^\varepsilon(x,\partial F)\,\mathrm{d}x \geq \frac{C\varepsilon}{\tau} > P_\varepsilon(E_0^{\tau,\varepsilon}).$$

This suggests that the meaningful regime is when $\tau/\varepsilon \to \gamma \in (0,+\infty)$, and we will focus on this case in the next Section.

3. Motion of an origin-symmetric convex "Wulff-like" set

We introduce a class of sets, the convex "Wulff-like" sets, for which the motion by crystalline curvature exists and is unique (at least) until the length of some side approaches to zero, and it is governed by a system of ordinary differential equations. Roughly speaking, a convex Wulff-like set has a polygonal boundary that is a 'good curve' containing only regular corners, according to J. Taylor's terminology [37, 2]; i.e., a convex set whose sides have the same exterior unit normal vectors and form the same angles as those of the Wulff shape $\mathcal{W}_{hex}$ of the density φ_{hex}. According to Lemma A.1(iii), the Wulff shape $\mathcal{W}_{hex}$ is the regular hexagon

$$\mathcal{W}_{hex} = \{\varphi^\circ_{hex} \leq 1\} = \frac{4}{3}\,\mathrm{conv}(\pm\eta_1, \pm\eta_2, \pm\eta_3)\,,$$

as pictured in Fig. 4. To simplify the notation, we relabel in clockwise order

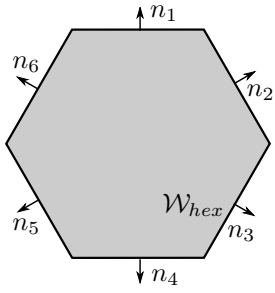

Figure 4. The Wulff shape $\mathcal{W}_{hex}$ of φ_{hex} is a regular hexagon.

the exterior unit normal vectors of the Wulff shape $\mathcal{W}_{hex}$ and we set

$$\mathcal{N} := \{n_1, n_2, n_3, n_4, n_5, n_6\}, \tag{3.1}$$

where $n_1 := \eta_1^\perp$, $n_2 := \eta_3^\perp$, $n_3 := -\eta_2^\perp$, $n_4 := -n_1$, $n_5 := -n_2$, $n_6 := -n_3$.

Definition 3.1 (Wulff-like set). A bounded set $E \subset \mathbb{R}^2$ is said to be *Wulff-like* if its boundary ∂E is a polygonal closed curve whose sides $S_i, i = 1, \dots, m$ have exterior unit normal vectors ν_i such that

(1) $\nu_i \in \mathcal{N}$, for every $i = 1, \dots, m$;
(2) if $\nu_i = n_j$ for some $j = 1, \dots, 6$, then $\nu_{i+1} \in \{n_{j-1}, n_{j+1}\}$.

Here, the labellings of ν_i and n_j are intended to be modulo m and 6, respectively.

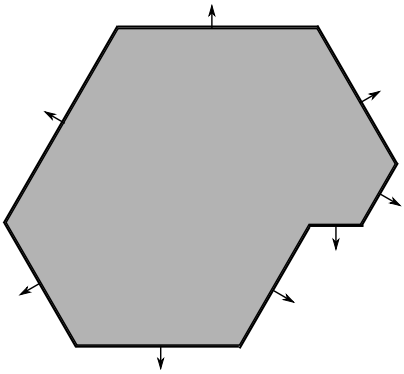

Figure 5. An example of Wulff-like set.

Equivalently, each pair of adjacent sides of a Wulff-like set forms either a *regular* or an *inverse corner*, according to the definition given in [2, Section 4]. In particular, each side is parallel to a side of the Wulff shape. Moreover, as an easy remark we note that *convex* Wulff-like sets are convex Wulff-like hexagons. Among these, origin-symmetric convex Wulff-like hexagons will play the same role of rectangles on the square lattice in [17], and we will see that this case contains the main features of the motion.

In view of (1.4)-(1.5), the weighted crystalline curvature of a side with length L is given by

$$M\kappa := -\frac{8}{\sqrt{3}L}\,. \tag{3.2}$$

Indeed, the natural mobility M of a side is independent of its normal vector n_i being $M(n_i) = \varphi_{hex}(n_i) \equiv M := \frac{2}{\sqrt{3}}$, and the side-length of the Wulff shape is $\Lambda(n_i) \equiv \Lambda := \frac{4}{3}$. Note that the evolution of more general (non-convex) sets may be studied up to assign a curvature sign on each side (see [17, Sections 3.2-3.3]). Namely, sides with a non-zero curvature may move outwards/inwards (according to the chosen convention on the sign of curvature), while sides with curvature 0 do not move (even if their lengths may decrease due to the motion of adjacent sides).

We will restrict the minimization of the energy $\mathcal{F}_{\tau,\varepsilon}$ defined in (2.7) to those sets in $\mathcal{D}_\varepsilon$ that are the union of all the cells of the hexagonal lattice strictly contained in a given convex Wulff-like hexagon. With a slight abuse of notation, we call such sets *discrete* convex Wulff-like hexagons.

Definition 3.2 (discrete convex Wulff-like hexagon). Let $\mathcal{D}_\varepsilon$ be defined as in (2.2). A set $E \in \mathcal{D}_\varepsilon$ is said to be a *discrete convex Wulff-like hexagon* if there exists a convex Wulff-like hexagon K such that

$$E = \bigcup_i \big\{ H_\varepsilon(i) : \, H_\varepsilon(i) \subset K \big\}.$$

We denote this subclass by $\widetilde{\mathcal{D}}_\varepsilon$.

Definition 3.3 (Wulff-like envelope). Given any $E \in \widetilde{\mathcal{D}}_\varepsilon$, we define $\mathcal{W}(E)$ the *Wulff-like envelope* of E as the smallest convex Wulff-like hexagon containing E.

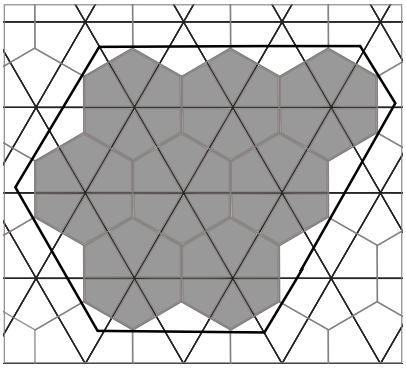

Figure 6. An example of discrete convex Wulff-like set.

An example of discrete convex Wulff-like hexagon is pictured in Fig. 6. The set is coloured in gray, while the continuous black line represents the boundary of its Wulff-like envelope.

Let $\tau = \tau(\varepsilon)$. We characterize the microscopic motion of discrete convex Wulff-like hexagons under the simplifying assumption that

$$\tau = \gamma\varepsilon \quad \text{ for some fixed } \gamma > 0\,,$$

the analysis at the critical regime $\tau \sim \gamma\varepsilon$ only requiring minor changes in the proof. Correspondingly, we omit the dependence on τ in the notation of $E_k^{\tau,\varepsilon} = E_k^{\gamma\varepsilon,\varepsilon}$ and $\mathcal{F}_{\tau,\varepsilon} = \mathcal{F}_{\gamma\varepsilon,\varepsilon}$, that will be simply denoted by E_k^ε and $\mathcal{F}_\varepsilon$, respectively.

The main result is that discrete *origin-symmetric* convex Wulff-like hexagons evolve into sets of the same type. This is the content of Proposition 3.4, whose proof is reminiscent of some geometric arguments developed in [17, Theorem 1] for rectangular evolutions with underlying square lattice. However, we have to face some technical difficulties due to the geometry of

the triangular lattice, as the fact that the boundary of a set in $\widetilde{\mathcal{D}}_\varepsilon$ and that of its Wulff-like envelope do not coincide.

Proposition 3.4. *If $E_0^\varepsilon \in \widetilde{\mathcal{D}}_\varepsilon$ is a discrete origin-symmetric convex Wulff-like hexagon and E_k^ε is a minimizer for the minimum problem for $\mathcal{F}_\varepsilon(\cdot, E_{k-1}^\varepsilon), k \geq 1$, then E_k^ε is a discrete origin-symmetric convex Wulff-like hexagon contained in E_{k-1}^ε as long as all the sides of its Wulff-like envelope $\mathcal{W}(E_{k-1}^\varepsilon)$ have strictly positive length.*

Proof. The existence of minimizers among the sets of finite perimeter relies on classical results of compactness and semicontinuity (see, e.g., [3, Section 3.2]). Here we characterize the geometrical properties of a minimizer. For this, it will suffice to show the assertion for $F = E_1^\varepsilon$ a minimizer of $\mathcal{F}_\varepsilon(\cdot, E_0^\varepsilon)$, since the general case will follow by induction on the step k. In order to do that, let $F = F_1 \cup \cdots \cup F_m$, $m \geq 1$, be the decomposition of F into its connected components.

Step 1: each F_i is a discrete convex Wulff-like hexagon contained in E_0^ε. First, we characterize each connected component of E_1^ε. We note that $E_1^\varepsilon \subseteq E_0^\varepsilon$. If not, let F_i be a connected component of E_1^ε such that $F_i \cap (E_0^\varepsilon)^c \neq \emptyset$; if $F_i \subseteq (E_0^\varepsilon)^c$, then we may strictly reduce the energy $\mathcal{F}_\varepsilon(\cdot, E_0^\varepsilon)$ simply by dropping it. If not, we could consider as a competitor the set $F_i \cap E_0^\varepsilon$: the area of the symmetric difference with E_0^ε clearly decreases and the same holds for the perimeter, since any external connected curve made by cell sides connecting any two points of $\partial F_i \cap \partial \mathcal{W}(E_0^\varepsilon)$ and containing cell sides orthogonal to $\partial \mathcal{W}(E_0^\varepsilon)$ has perimeter not smaller than the one determined by the path along ∂E_0^ε (see Fig. 7).

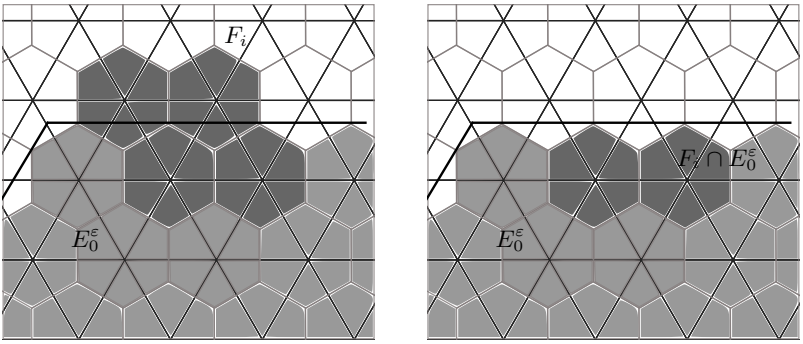

Figure 7. Each F_i is contained in E_0^ε.

Now, if F_i is a discrete convex Wulff-like hexagon, then we are done. If not, we replace each F_i with the smallest discrete convex Wulff-like hexagon containing F_i; in this case, its energy decreases since its perimeter is not greater than that of F_i and the symmetric difference with E_0^ε decreases as well (see Fig. 8). More precisely, if we define

$$\widetilde{F}_i = \cup_j \{H_\varepsilon(j) : H_\varepsilon(j) \subseteq \mathcal{W}(F_i)\},$$

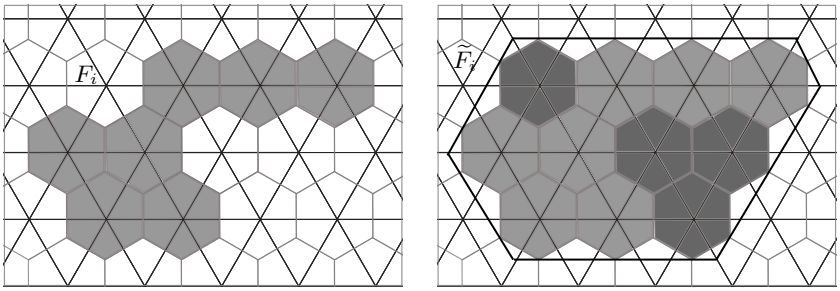

Figure 8. The Wulff-like "convexification" of F_i reduces both its perimeter and the symmetric difference with the previous set.

since $F_i \subseteq \widetilde{F}_i \subseteq E_0^\varepsilon$ we immediately get that $\mathcal{L}^2(\widetilde{F}_i \triangle E_0^\varepsilon) \leq \mathcal{L}^2(F_i \triangle E_0^\varepsilon)$. In addition, we claim that $P_\varepsilon(\widetilde{F}_i) \leq P_\varepsilon(F_i)$. For this, we consider the intersection of $\partial\widetilde{F}_i$ with a side S_j of $\mathcal{W}(F_i)$ having normal vector $\pm\eta_j^\perp$, for some $j = 1, 2, 3$. Such an intersection will contain at least one point belonging to $\partial F_i \cap \partial\widetilde{F}_i$. Each connected curve made by cell sides passing through such points and different from the corresponding path along $\partial\widetilde{F}_i$ would contain some cell side (orthogonal to S_j) with normal vector $\pm\eta_j$, thus increasing the perimeter.

Step 2: each F_i can be translated towards the origin without increasing its energy. We rewrite the bulk term in the energy (2.7) as

$$\begin{aligned}
\int_{F \triangle E_0^\varepsilon} d^\varepsilon(x, \partial E_0^\varepsilon)\,\mathrm{d}x &= \int_{E_0^\varepsilon \setminus F} d^\varepsilon(x, \partial E_0^\varepsilon)\,\mathrm{d}x \\
&= \int_{E_0^\varepsilon} d^\varepsilon(x, \partial E_0^\varepsilon)\,\mathrm{d}x - \int_F d^\varepsilon(x, \partial E_0^\varepsilon)\,\mathrm{d}x \\
&= \int_{E_0^\varepsilon} d^\varepsilon(x, \partial E_0^\varepsilon)\,\mathrm{d}x - \int_{\cup_{i=1}^m F_i} d^\varepsilon(x, \partial E_0^\varepsilon)\,\mathrm{d}x \\
&= \int_{E_0^\varepsilon} d^\varepsilon(x, \partial E_0^\varepsilon)\,\mathrm{d}x - \sum_{i=1}^m \int_{F_i} d^\varepsilon(x, \partial E_0^\varepsilon)\,\mathrm{d}x\,,
\end{aligned}$$

where in the latter equality the first integral is a fixed quantity independent of F and the second negative term can be either reduced or left unchanged by replacing each component F_i with a suitable translation of F_i towards the origin.

We consider the component F_1. We can suppose that $O \notin F_1$, since there is at most one connected component of F containing O. By the symmetry of $\mathcal{W}(E_0^\varepsilon)$, we can consider and fix any of its axes of symmetry r passing through O, and by the discrete convexity of F_1, we may assume that $\mathcal{W}(F_1)$ is entirely contained in any of the half-planes determined by r (see Fig. 9). We define the set F' obtained by substituting to F_1 any of its translations towards O, say F_1', resulting from the composition of a finite number of translations of F_1 pointing to O (see Fig. 9 (a_1)-(a_3)), so that the distance $d^\varepsilon(\cdot, \partial E_0^\varepsilon)$ is nondecreasing pointwise on F_1 and thence the bulk term in the energy does

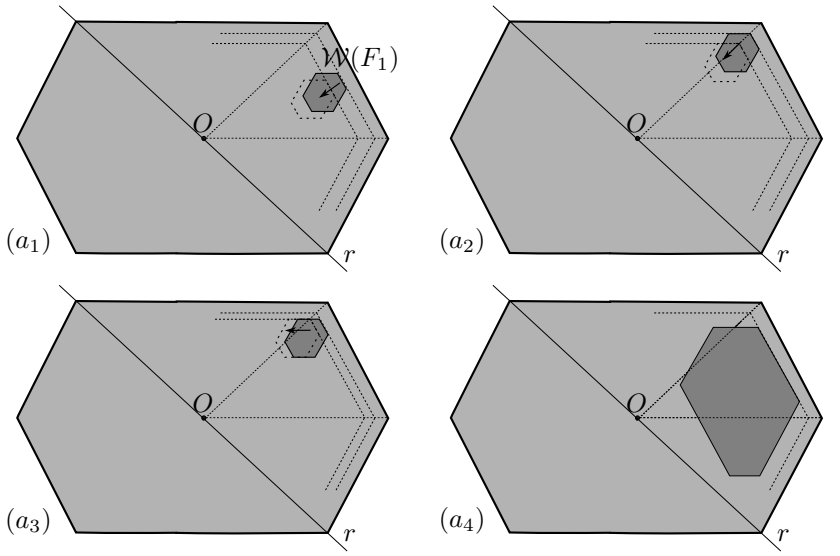

Figure 9. The translations of F_1 towards O not increasing the bulk term of the energy.

not increase; equivalently,

$$\int_{F_1'} d^\varepsilon(x, \partial E_0^\varepsilon)\,\mathrm{d}x \geq \int_{F_1} d^\varepsilon(x, \partial E_0^\varepsilon)\,\mathrm{d}x\,. \tag{3.3}$$

For the sake of simplicity, we argue on the Wulff-like envelopes of E_ε^0 and F_1. We distinguish between different cases: (i) all the points of $\mathcal{W}(F_1)$ project onto the same side of $\mathcal{W}(E_0^\varepsilon)$, with normal vector n, and $d^\varepsilon(F_1, \partial E_\varepsilon^0) = \frac{3}{4}q\varepsilon$ for some $q \in \mathbb{N}$; (ii) the points of $\mathcal{W}(F_1)$ project onto a pair of consecutive sides of $\mathcal{W}(E_0^\varepsilon)$, and the distance to both the sides is the same; (iii) $\mathcal{W}(F_1)$ projects onto a pair of consecutive sides of $\mathcal{W}(E_0^\varepsilon)$ and the distances from the sides are different, say $\frac{3}{4}q_1\varepsilon$ and $\frac{3}{4}q_2\varepsilon$, for some $q_1, q_2 \in \mathbb{N}$ with $q_1 < q_2$. In case (i), to define F_1' it will suffice to consider the minimal translation δ of F_1 in the direction $-n$ to get $d^\varepsilon(F_1', \partial E_0^\varepsilon) = \frac{3}{4}(q+1)\varepsilon > d^\varepsilon(F_1, \partial E_\varepsilon^0)$ (see Fig. 9 (a_1)). Indeed, setting $x' = \delta(x)$, this implies that

$$d^\varepsilon(x', \partial E_\varepsilon^0) \geq d^\varepsilon(x, \partial E_\varepsilon^0)\,,\ \text{for every } x \in F_1,$$

whence (3.3) immediately follows. In situation (ii), F_1' can be defined by translating F_1 towards O along the axis of symmetry intersecting F_1, thus increasing the distance of the component to both the sides of $\mathcal{W}(E_\varepsilon^0)$ (Fig. 9 (a_2)). As for (iii), F_1 can be translated in the lattice directions (alongside the level sets of the distance to the boundary) in such a way to leave unchanged the distance of the component to the farthest side and to increase the distance to the nearest one (see Fig. 9 (a_3)), thus obtaining $d^\varepsilon(F_1', \partial E_0^\varepsilon) = \frac{3}{4}q_2\varepsilon$. Now, the bulk term can be further reduced, if necessary, by arguing as in (ii).

Eventually, for a "big" component as in Fig. 9 (a_4), an energy reducing translation can be obtained as the composition of a finite number of translations as in (i), (ii) and (iii).

The perimeter of F_1' is the same as that of F_1, hence the perimeter term of $\mathcal{F}_\varepsilon(F', E_0^\varepsilon)$ remains unchanged, unless the boundary of F_1' intersects the boundary of some other F_j, $j \neq 1$, for a positive length (in which case the energy strictly decreases).

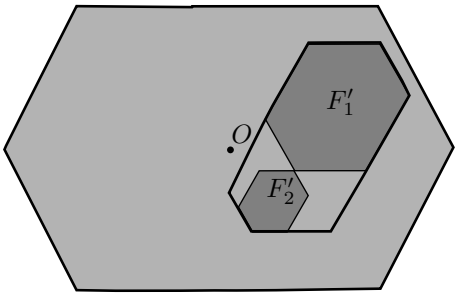

Figure 10. The components F_1' and F_2' intersect in a common corner. In this case, the smallest discrete convex Wulff-like hexagon containing $F_1' \cup F_2'$ is a competitor with less energy.

Step 3: F is connected. If $m = 1$ there is nothing to prove, so we assume that $m \geq 2$. In this case, the translation argument of Step 2, applied to F_1 and F_2, after a finite number of steps produces a competitor F' where the boundaries of two such translated connected components, say F_1' and F_2', touch. Then their boundaries intersect either in a set of positive length (a cell side), in which case a cancelation gives a lower contribution of the perimeter, or in a common corner, in which case we can further consider the competitor F'' obtained by substituting $F_1' \cup F_2'$ with the smallest discrete convex Wulff-like hexagon containing $F_1' \cup F_2'$ (see Fig. 10), for which the energy decreases as shown in Step 1. In both the cases, we obtain a contradiction with the minimality of F. Hence, any minimizer F has only one connected component, which is a discrete convex Wulff-like hexagon.

Step 4: F contains the origin O. If not, we may consider the discrete convex Wulff-like hexagon $\widetilde{F}$ being the reflection of F with respect to the origin (see Fig. 11). In this case, we have $P_\varepsilon(\widetilde{F}) = P_\varepsilon(F)$ and, by the symmetry of E_0^ε, $\int_{\widetilde{F} \triangle E_0^\varepsilon} d^\varepsilon(x, \partial E_0^\varepsilon)\,\mathrm{d}x = \int_{F \triangle E_0^\varepsilon} d^\varepsilon(x, \partial E_0^\varepsilon)\,\mathrm{d}x$. Moreover, a comparison between the values $\mathcal{F}_\varepsilon(F, E_0^\varepsilon)$ and $\mathcal{F}_\varepsilon(\emptyset, E_0^\varepsilon)$ gives

$$P_\varepsilon(F) \leq \frac{1}{\tau} \int_F d^\varepsilon(x, \partial E_0^\varepsilon)\,\mathrm{d}x,$$

whence

$$\mathcal{F}_\varepsilon(\widetilde{F} \cup F, E_0^\varepsilon) = \mathcal{F}_\varepsilon(F, E_0^\varepsilon) + P_\varepsilon(F) - \frac{1}{\tau} \int_{\widetilde{F}} d^\varepsilon(x, \partial E_0^\varepsilon)\,\mathrm{d}x \leq \mathcal{F}_\varepsilon(F, E_0^\varepsilon).$$

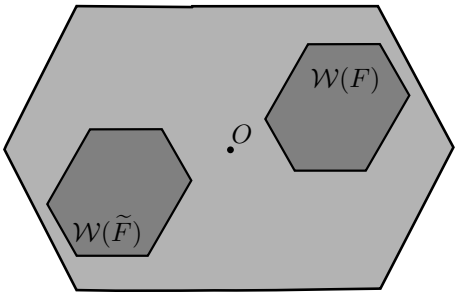

Figure 11. F and its reflection $\widetilde{F}$ with respect to O. The set $F \cup \widetilde{F}$ is a competitor with less energy than F.

Thus, $\widetilde{F} \cup F$ is also a minimizer, and this contradicts the connectedness of the minimizer provided by Step 3.

Step 5: explicit computation of E_1^ε. Let $L_i^\varepsilon := \mathcal{H}^1(S_i^{0,\varepsilon})$ be the length of the i-th side $S_i^{0,\varepsilon}$ of $\mathcal{W}(E_0^\varepsilon)$, $S_i^{1,\varepsilon}$ be the i-th side of $\mathcal{W}(E_1^\varepsilon)$ and $L_i^{1,\varepsilon}$ its length, $\frac{\sqrt{3}}{2}\varepsilon\overline{N}_i$, with $\overline{N}_i$ integer, and s_i^ε be the distances of the side $S_i^{1,\varepsilon}$ from $S_i^{0,\varepsilon}$ and O, respectively. If we subdivide the area between $S_i^{1,\varepsilon}$ and $S_i^{0,\varepsilon}$ in $\overline{N}_i$ layers of $L_i^\varepsilon/\varepsilon$ hexagonal cells indexed by k, for each of which the discrete distance from the boundary is $\frac{3}{4}k\varepsilon$, we can write the functional $\mathcal{F}_\varepsilon(\cdot, E_0^\varepsilon)$ in terms of the integers N_i, and we get that $\overline{N}_1, \overline{N}_2, \dots, \overline{N}_6$ are the minimizers of the function

$$\begin{aligned} f(N_1, N_2, \dots, N_6) &= -\frac{2\sqrt{3}}{3}\varepsilon \sum_{i=1}^{6} N_i + \frac{\varepsilon^2}{\tau}\sum_{i=1}^{6}\sum_{k=1}^{N_i}\frac{3}{4}(k\varepsilon)\frac{L_i^\varepsilon}{\varepsilon}\frac{\sqrt{3}}{2} - \frac{\varepsilon^2}{\gamma}e_\varepsilon \\ &= \sqrt{3}\varepsilon\sum_{i=1}^{6}\left(-\frac{2}{3}N_i + \frac{3}{8\gamma}\frac{N_i(N_i+1)}{2}L_i^\varepsilon\right) - \frac{\varepsilon^2}{\gamma}e_\varepsilon, \end{aligned} \tag{3.4}$$

with $0 < e_\varepsilon \le C\max(\overline{N}_1, \dots, \overline{N}_6)^3$. The error e_ε is due to the bulk contribution of the hexagonal cells near the vertices of $S_{i,\varepsilon}$, which is negligible as $\varepsilon \to 0$.

The minimizer of (3.4) is characterized by the inequalities

$$f(\dots, \overline{N}_i, \dots) \le f(\dots, \overline{N}_i \pm 1, \dots), \quad i = 1, \dots, 6.$$

Setting $\alpha_{hex} := \frac{16}{9}$, since $f(\dots, N_i, \dots)$ is a parabola, the optimal value $\overline{N}_i$ of N_i is the integer closest to

$$\frac{\alpha_{hex}\gamma}{L_i^\varepsilon} - \frac{1}{2},$$

that is, $\overline{N}_i = \left\lfloor \frac{\alpha_{hex}\gamma}{L_i^\varepsilon} \right\rfloor$ unless $\frac{\alpha_{hex}\gamma}{L_i^\varepsilon}$ lies in a small neighborhood of the integers, infinitesimal as $\varepsilon \to 0$, when both an integer and the subsequent one are minimizers (see Section 3.3 for a discussion). We convene that

$$\text{if } L_i^\varepsilon = L_j^\varepsilon \text{ for } i \neq j, \text{ then } \overline{N}_i = \overline{N}_j\,. \tag{3.5}$$

Clearly, (3.5) is significant when $\overline{N}_i$ is not uniquely determined by L_i^ε, and amounts to assign the same discrete velocity, once it has been chosen, to sides with the same discrete length. We then have

$$s_i^{1,\varepsilon} = s_i^\varepsilon - \tfrac{\sqrt{3}}{2}\overline{N}_i\varepsilon, \tag{3.6}$$

$$L_i^{1,\varepsilon} = L_i^\varepsilon + \big(\overline{N}_i - (\overline{N}_{i-1} + \overline{N}_{i+1})\big)\varepsilon, \tag{3.7}$$

where, by the symmetry assumption on E_0^ε and (3.5), $\overline{N}_1 = \overline{N}_4$, $\overline{N}_2 = \overline{N}_5$ and $\overline{N}_3 = \overline{N}_6$, thus giving $L_1^{1,\varepsilon} = L_4^{1,\varepsilon}$, $L_2^{1,\varepsilon} = L_5^{1,\varepsilon}$ and $L_3^{1,\varepsilon} = L_6^{1,\varepsilon}$. In particular, E_1^ε is origin-symmetric.

The previous construction can be iterated recursively for $k > 1$, as long as $\mathcal{W}(E_{k-1}^\varepsilon)$ remains an hexagon; that is, the length of each side of $\mathcal{W}(E_{k-1}^\varepsilon)$ is strictly positive. □

In the following sections, we will focus on the description of any limit evolution.

3.1. The pinning threshold

We first examine the case when the limit motion is trivial; i.e., all E_k^ε are the same after a finite number of steps, thus giving the same set in the limit for each time. In case of rectangular evolutions with underlying lattice $\varepsilon\mathbb{Z}^2$ (see [17, Remark 3], [20, Section 3.1]), this is done by computing the *pinning threshold*; i.e., the critical value of the side length L above which it is energetically not favorable for a side to move. This is obtained by imposing that the minimal displacement of a side by ε along any of the coordinate directions e_1, e_2 gives a non-negative contribution in the energy.

Also in our setting the coordinate directions of the underlying lattice coincide with the 'preferred' directions for the motion $\{n_i,\, i = 1, \dots, 6\}$. The microscopic motion of a side is obtained by overcoming energy barriers along its normal direction; thus, the pinning threshold can be defined as *the critical value $\overline{L}$ for the length of a side of the initial limit set above which it is not energetically favorable for such a side to move.*

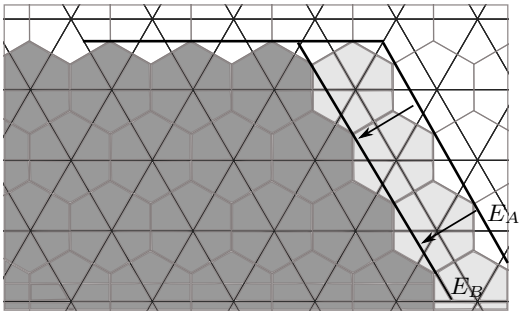

Figure 12. The minimal displacement of a side along its normal direction.

In order to determine it, we write the variation of the energy functional $\mathcal{F}_\varepsilon$ from configuration E_A to configuration E_B in Fig. 12, regarding the inward translation by $\frac{\sqrt{3}}{2}\varepsilon$ of a side of length L along its normal direction; this consists in computing the variation of the energy corresponding to the removal of the layer of hexagonal cells coloured in light gray. If we impose it to be positive, we get

$$\begin{aligned} P_\varepsilon(E_B) - P_\varepsilon(E_A) + \frac{3}{4\tau}\mathcal{L}^2(E_A \backslash E_B)\varepsilon &= -\frac{2\sqrt{3}}{3}\varepsilon + \frac{3}{4\gamma\varepsilon}\Big(\frac{L}{\varepsilon}\frac{\sqrt{3}}{2}\varepsilon^2\Big)\varepsilon \\ &= \sqrt{3}\varepsilon\left[-\frac{2}{3} + \frac{3}{8}\frac{L}{\gamma}\right] \geq 0, \end{aligned}$$

whence we deduce that

$$L \geq \overline{L} = \alpha_{hex}\gamma\,. \tag{3.8}$$

3.2. Description of the limit motion.

With the result of Proposition 3.4 at hand, we are now able to provide the characterization of any limit motion in the regime $\tau = \gamma\varepsilon$ for the class of origin-symmetric convex Wulff-like hexagons. The restriction to this class ensures more symmetry for the motion. Indeed, with the following Theorem 3.5, we prove the convergence of the discrete scheme (2.7), as $\varepsilon \to 0$, to a limit evolution which is a set of the same type for each time, until the length of any of its sides vanishes. In particular, a regular Wulff-like hexagon shrinks homothetically until the extinction time. Among the main features of the limit evolutions due to the discrete motion described at Step 5 of the proof of Proposition 3.4 and in Section 3.1, we retrieve the phenomenon of "quantization" of the velocities. In other words, we expect velocities depending in a discontinuous way on the curvature and (possibly) not always uniquely determined.

Theorem 3.5. *For all $\varepsilon > 0$, let $E_0^\varepsilon \in \widetilde{\mathcal{D}}_\varepsilon$ be discrete origin-symmetric convex Wulff-like hexagons and let the corresponding Wulff-like envelopes $\mathcal{W}(E_0^\varepsilon)$ have sides $S^0_{1,\varepsilon}, \dots, S^0_{6,\varepsilon}$. Assume also that*

$$\mathrm{d}_{\mathcal{H}}(\mathcal{W}(E_0^\varepsilon), E_0) < \varepsilon \tag{3.9}$$

for some fixed origin-symmetric convex Wulff-like hexagon E_0. Let $\gamma > 0$ be fixed, $E^\varepsilon(t) := \mathcal{W}(E^\varepsilon_{\lfloor t/\gamma\varepsilon \rfloor})$ be the Wulff-like envelope of $E^\varepsilon_{\lfloor t/\gamma\varepsilon \rfloor}$ the piecewise-constant motion with initial datum E_0^ε defined in (2.8)*. Then there exists $T > 0$ such that $E^\varepsilon(t)$ converges, up to a subsequence, as $\varepsilon \to 0$, in the Hausdorff topology and locally uniformly on $[0, T)$, to an origin-symmetric convex Wulff-like hexagon $E(t)$ with sides $S_i(t), i = 1, \dots, 6$ and such that $E(0) = E_0$. The distance $s_i(t)$ of the side $S_i(t)$ from the origin O reduces*

with a velocity $v_i(t)$ satisfying

$$v_i(t)\begin{cases} = \dfrac{\sqrt{3}}{2}\Big(\dfrac{1}{\gamma}\left\lfloor\dfrac{\alpha_{hex}\gamma}{L_i(t)}\right\rfloor\Big), & \text{if } \dfrac{\alpha_{hex}\gamma}{L_i(t)} \notin \mathbb{N} \\ \in \dfrac{\sqrt{3}}{2}\left[\dfrac{1}{\gamma}\left(\dfrac{\alpha_{hex}\gamma}{L_i(t)}-1\right), \dfrac{\alpha_{hex}}{L_i(t)}\right], & \text{if } \dfrac{\alpha_{hex}\gamma}{L_i(t)} \in \mathbb{N}. \end{cases} \tag{3.10}$$

where $L_i(t) := \mathcal{H}^1(S_i(t))$ denotes the length of the side $S_i(t)$. Accordingly, the law for each $L_i(t)$ is

$$\dot{L}_i(t) = \frac{2}{\sqrt{3}}\left[v_i(t) - (v_{i-1}(t) + v_{i+1}(t))\right], \quad i = 1, \dots, 6, \tag{3.11}$$

with the convention that symbols v_i and v_j coincide if $i \equiv j$ modulo 6.

Before entering into details of the proof, we note that a natural choice for $T > 0$ (see [17, Theorem 3]) is the first time for which $\lim_{t\to T^-} L_i(t) = 0$ for some $i \in \{1, 2, \dots, 6\}$. If on the one hand it is worth mentioning that an extension of the crystalline motion for times past such T, consisting of both deleting vanishing sides and possibly merging some other sides, has been provided in [37, Section 2.3], on the other hand we note that an analogous delicate construction in the discrete setting would be out of this paper's scope. Thus, we agree that the evolution of a convex Wulff-like hexagon exists until one of its sides vanishes.

Proof of Theorem 3.5. In view of Proposition 3.4, each E_k^ε, $k \geq 1$, is a discrete origin-symmetric convex Wulff-like hexagon contained in E_{k-1}^ε. We determine here explicitly the minimizer E_k^ε, by iterating recursively at each step $k > 1$ an analogous computation as done for $k = 1$ at Step 5 of the proof of Proposition 3.4. Namely, for $k \geq 1$ and $i = 1, \dots, 6$ we construct three sequences $s_i^{k,\varepsilon}$, $L_i^{k,\varepsilon}$ and $N_i^{k,\varepsilon}$ such that

$$s_i^{k+1,\varepsilon} = s_i^{k,\varepsilon} - \tfrac{\sqrt{3}}{2} N_i^{k,\varepsilon}\varepsilon, \tag{3.12}$$

$$L_i^{k+1,\varepsilon} = L_i^{k,\varepsilon} + \tfrac{2}{\sqrt{3}}\big(s_{i+1}^{k+1,\varepsilon} - s_{i+1}^{k,\varepsilon} + s_{i-1}^{k+1,\varepsilon} - s_{i-1}^{k,\varepsilon} + s_i^{k,\varepsilon} - s_i^{k+1,\varepsilon}\big) \tag{3.13}$$

since by geometry there holds (see, e.g., [37, p. 423])

$$\begin{aligned} L_i^{k,\varepsilon} &= \frac{s_{i+1}^{k,\varepsilon} - \langle n_{i+1}, n_i\rangle s_i^{k,\varepsilon}}{\sqrt{1 - (\langle n_{i+1}, n_i\rangle)^2}} + \frac{s_{i-1}^{k,\varepsilon} - \langle n_{i-1}, n_i\rangle s_i^{k,\varepsilon}}{\sqrt{1 - (\langle n_{i-1}, n_i\rangle)^2}} \\ &= \frac{2}{\sqrt{3}}\big(s_{i+1}^{k,\varepsilon} + s_{i-1}^{k,\varepsilon} - s_i^{k,\varepsilon}\big), \end{aligned} \tag{3.14}$$

where $s_i^{1,\varepsilon}$, $L_i^{1,\varepsilon}$ have been already determined in (3.6)-(3.7) with initial conditions $s_i^{0,\varepsilon} = s_i^\varepsilon$, $N_i^{0,\varepsilon} = \overline{N}_i$ and $L_i^{0,\varepsilon} = L_i^\varepsilon$, $\overline{N}_i$ resulting by the minimization of (3.4). In (3.12), $N_i^{k,\varepsilon}$ is a minimizer of

$$f(N_1, N_2, \dots, N_6) = \sqrt{3}\varepsilon \sum_{i=1}^{6}\left(-\frac{2}{3}N_i + \frac{3}{8\gamma}\frac{N_i(N_i+1)}{2}L_i^{k,\varepsilon}\right) - \frac{\varepsilon^2}{\gamma}e_\varepsilon. \tag{3.15}$$

For each $1 \leq i \leq 6$, we define $\bar{s}_i^\varepsilon(t)$ and $\bar{L}_i^\varepsilon(t)$ to be the piecewise affine interpolations in $[k\tau,(k+1)\tau]$ of the values $s_i^{k,\varepsilon}$ and $L_i^{k,\varepsilon}$, respectively. From (3.13) we deduce the identity

$$\bar{L}_i^\varepsilon(t) = L_i^{0,\varepsilon} + \frac{2}{\sqrt{3}}(s_i^{0,\varepsilon} - \bar{s}_i^\varepsilon(t) - (s_{i-1}^{0,\varepsilon} - \bar{s}_{i-1}^\varepsilon(t) + s_{i+1}^{0,\varepsilon} - \bar{s}_{i+1}^\varepsilon(t))). \quad (3.16)$$

Let $T_\varepsilon > 0$ be defined as

$$T_\varepsilon := \sup\left\{t > 0 : \exists c > 0 \text{ such that } \bar{L}_i^\varepsilon(r) \geq c, \quad \forall r \in [0,t), \text{ for every } i\right\},$$

and let $\overline{T} \in (0, T_\varepsilon)$ be arbitrarily fixed. By (3.12) we have

$$\frac{s_i^{k+1,\varepsilon} - s_i^{k,\varepsilon}}{\tau} = -\frac{\sqrt{3}}{2\gamma} N_i^{k,\varepsilon}, \quad (3.17)$$

so that $\bar{s}_i^\varepsilon(t)$ is a decreasing continuous function of t. Since by (3.9) we may assume that $|s_i^{0,\varepsilon} - s_i^0| \leq c\varepsilon$ for every i and a suitable constant c, the monotonicity of $\bar{s}_i^\varepsilon(t)$ implies the existence of $\varepsilon_0 > 0$ and a uniform constant $C_1 > 0$ such that

$$|\bar{s}_i^\varepsilon(t)| \leq C_1, \quad \text{for every } t \in [0,\overline{T}], \text{ for } \varepsilon \leq \varepsilon_0. \quad (3.18)$$

Moreover, it holds that

$$|\bar{s}_i^\varepsilon(t_1) - \bar{s}_i^\varepsilon(t_2)| \leq C_2|t_1 - t_2|, \quad \text{for every } t_1, t_2 \in [0,\overline{T}], \quad (3.19)$$

for some positive constant C_2 independent of ε. In order to prove this, we may assume that $t_2 < t_1$. Then, taking into account (3.17), we get

$$\begin{aligned}
&|\bar{s}_i^\varepsilon(t_1) - \bar{s}_i^\varepsilon(t_2)| \\
&\leq |\bar{s}_i^\varepsilon(t_1) - s_i^{\lfloor t_1/\tau\rfloor,\varepsilon}| + \sum_{r=\lfloor t_2/\tau\rfloor+1}^{\lfloor t_1/\tau\rfloor-1} |s_i^{r+1,\varepsilon} - s_i^{r,\varepsilon}| + |s_i^{\lfloor t_2/\tau\rfloor+1,\varepsilon} - \bar{s}_i^\varepsilon(t_2)| \\
&\leq \frac{\sqrt{3}}{2\gamma}\left[(t_1 - \lfloor t_1/\tau\rfloor\tau) + (\lfloor t_1/\tau\rfloor - \lfloor t_2/\tau\rfloor - 1)\tau + ((\lfloor t_2/\tau\rfloor + 1)\tau - t_2)\right] \\
&\leq \frac{\sqrt{3}}{2\gamma}|t_1 - t_2|.
\end{aligned}$$

Hence, in view of (3.18)-(3.19), by the Ascoli-Arzelà theorem there exists a subsequence $\bar{s}_i^{\varepsilon_j}(t)$, with $\varepsilon_j \to 0$, converging uniformly on $[0,\overline{T}]$, as $j \to +\infty$, to a continuous function $s_i(t)$, which is also decreasing. Moreover, with (3.16), we get the convergence of $\bar{L}_i^\varepsilon(t)$, as $\varepsilon_j \to 0$, to the function $L_i(t)$ defined as

$$L_i(t) := L_i^0 + \frac{2}{\sqrt{3}}(s_i^0 - s_i(t) - (s_{i-1}^0 - s_{i-1}(t) + s_{i+1}^0 - s_{i+1}(t))),$$

where we used also the fact that, by (3.9) and (3.14),

$$|L_i^{0,\varepsilon} - L_i^0| \leq \frac{\sqrt{3}}{2}(|s_i^{0,\varepsilon} - s_i^0| + |s_{i-1}^{0,\varepsilon} - s_{i-1}^0| + |s_{i+1}^{0,\varepsilon} - s_{i+1}^0|) \leq c'\varepsilon.$$

Setting

$$T := \sup\left\{t > 0 : L_i(r) > 0, \quad \forall r \in [0,t), \text{ for every } i\right\},$$

as a consequence of the convergence result, we have also that $\lim_j T_{\varepsilon_j} = T$. This allows us to choose $\overline{T}$ arbitrarily close to the extinction time T.
It follows that $E^{\varepsilon_j}(t)$ converges as $\varepsilon_j \to 0$, in the Hausdorff sense and locally uniformly on $[0,T)$, to the origin-symmetric convex Wulff-like hexagon $E(t)$ with sides of lengths $L_i(t)$, $i = 1, 2, \dots, 6$, such that $E(0) = E_0$.

Now we justify the formula (3.10) for the velocities. To simplify the computation, we introduce the piecewise-constant interpolations of the values $s_i^{k,\varepsilon}, L_i^{k,\varepsilon}, N_i^{\varepsilon}$; namely, for $t \geq 0$ we put $s_i^\tau(t) = s_i^{\lfloor t/\tau \rfloor, \varepsilon}$, $L_i^\tau(t) = L_i^{\lfloor t/\tau \rfloor, \varepsilon}$ and $N_i^\tau(t) = N_i^{\lfloor t/\tau \rfloor, \varepsilon}$. Note that, if $\varepsilon, \tau \to 0$, then

$$\bar{s}_i^\varepsilon(t) - s_i^\tau(t) \to 0, \qquad \text{uniformly with respect to } t \in [0, \overline{T}].$$

Indeed, for every $t \in [k\tau, (k+1)\tau]$, from (3.17) we have the estimate

$$|\bar{s}_i^\varepsilon(t) - s_i^\tau(t)| = \frac{|s_i^{k+1,\varepsilon} - s_i^{k,\varepsilon}|}{\tau} |t - k\tau| \leq |s_i^{k+1,\varepsilon} - s_i^{k,\varepsilon}| \leq \frac{\sqrt{3}}{2}\varepsilon.$$

Thus, $s_i^\tau(t) \to s_i(t)$, $L_i^\tau(t) \to L_i(t)$ locally uniformly as $\tau \to 0$ and, by continuity, $N_i^\tau(t) \to \frac{2\gamma v_i(t)}{\sqrt{3}}$ as $\tau \to 0$, where the velocities $v_i(t)$ are defined by (3.10). By construction we have

$$\begin{aligned} s_i^\tau(t+\tau) &= s_i^0 - \frac{\sqrt{3}}{2\gamma} \sum_{k=0}^{\lfloor t/\tau \rfloor} \tau N_i^\tau(k\tau) \\ &= s_i^0 - \sum_{k=0}^{\lfloor t/\tau \rfloor} \tau v_i(k\tau) + \omega(\tau), \end{aligned}$$

$\omega(\tau)$ being an infinitesimal error as $\tau \to 0$, where the second equality has been obtained using the convergence of N_i^τ to $\frac{2\gamma v_i(t)}{\sqrt{3}}$. Passing to the limit as $\tau \to 0$ we finally deduce that

$$s_i(t) = s_i^0 - \int_0^t v_i(s)\, ds,$$

that is equivalent to (3.10) rephrased through the relation $\dot{s}_i(t) = -v_i(t)$.

As for (3.11), from (3.13) and arguing as before we get

$$\begin{aligned} L_i^\tau(t+\tau) &= L_i^0 + \sum_{k=0}^{\lfloor t/\tau \rfloor} \tau [N_i^\tau(k\tau) - (N_{i-1}^\tau(k\tau) + N_{i+1}^\tau(k\tau))] \\ &= L_i^0 + \frac{2}{\sqrt{3}} \sum_{k=0}^{\lfloor t/\tau \rfloor} \tau [v_i(k\tau) - (v_{i-1}(k\tau) + v_{i+1}(k\tau))] + \omega(\tau), \end{aligned}$$

whence, passing to the limit as $\tau \to 0$, we obtain

$$L_i(t) = L_i^0 + \frac{2}{\sqrt{3}} \int_0^t v_i(s) - (v_{i-1}(s) + v_{i+1}(s))\, ds,$$

from which (3.11) follows by taking the time derivative of both the sides. □

The explicit description of the evolution (3.11) for any convex Wulff-like hexagon is tricky, since the rate of change of the length for each side depends on the velocities of the neighboring sides. Furthermore, according to the sign of the right hand side in (3.11), a side may shorten or lengthen, possibly reaching the pinning threshold after an initial motion. In this case, the uniqueness of velocities (3.10) may no longer hold.

The following theorem characterizes the limit evolutions of some initial data providing a unique choice for the velocities v_i in (3.10). That is the case, for instance, when (a) all the sides are pinned ("total pinning") and the motion is trivial; (b) all the sides have the same length and are short enough ("motion of a Wulff shape"), thus obeying to a self-similar evolution that extinguishes in finite time.

Theorem 3.6 (unique limit motions). *Let $E^\varepsilon(t), E_0$ be as in the statement of Theorem 3.5, and denote by $L_i^0, i = 1, \dots, 6$ the lengths of the sides of the initial set E_0. Then the following hold:*

(a) (total pinning) *if $\min_{1\le i\le 6}\{L_i^0\} > \alpha_{hex}\gamma$, $E^\varepsilon(t)$ converges as $\varepsilon \to 0$ to $E(t) \equiv E_0$ for every $t \ge 0$;*

(b) (self-similar evolution vanishing in finite time) *if $L_i^0 = L^0 < \alpha_{hex}\gamma$ for every $i = 1, \dots, 6$, then there exists $T > 0$ such that $E^\varepsilon(t)$ converges locally in time on $[0, T)$ as $\varepsilon \to 0$ to $E(t)$, where $E(t)$ is the unique regular Wulff-like hexagon with side-length $L(t)$ solution to the degenerate ordinary differential equation*

$$\dot{L}(t) = -\frac{1}{\gamma}\left\lfloor \frac{\alpha_{hex}\gamma}{L(t)} \right\rfloor , \tag{3.20}$$

for almost every $t \in [0, T)$, with initial condition $L(0) = L^0$.

Proof. (a) The assertion immediately follows from (3.10) noticing that we have $v_i(t) = 0$ for all $t \ge 0$, which is equivalent to $\dot{s}_i = 0$. Correspondingly, $\dot{L}_i(t) \equiv 0$.

(b) The law (3.20) is a consequence of (3.10)-(3.11), once we remark that $s_i(t) \equiv s(t)$ is independent of the sides and coincides with the apothem of $E(t)$, and it holds that $\dot{L}(t) = \frac{2}{\sqrt{3}}\dot{s}(t)$. According to (3.10), the side length $L(t)$ decreases, with a strictly negative derivative $\dot{L}(t) \le -1/\gamma$, until it vanishes. Thus, $\frac{\alpha_{hex}\gamma}{L(t)} \in \mathbb{N}$ only for a countable set $\mathcal{T}$ of times t and (3.20) immediately follows. The uniqueness for the solution of equation (3.20) can be proved by arguing on each subinterval outside $\mathcal{T}$, where uniqueness holds, and using the fact that $L(t)$ is uniquely determined for $t \in \mathcal{T}$. □

3.3. Quantized velocities, non-uniqueness and partial pinning

We give here an insight on the non-uniqueness of solutions, mentioned in the proof of Proposition 3.4, when minimizing the function (3.4) among the integers. As discussed in [17, p. 480], there exists a constant depending on the lengths of the limit sides, $\bar{C} = \bar{C}(L_1, \dots, L_6)$, such that the minimization problem has the unique solution $\overline{N}_i = \lfloor \frac{\alpha_{hex}\gamma}{L_i^\varepsilon} \rfloor$ if $\operatorname{dist}\left(\frac{\alpha_{hex}\gamma}{L_i^\varepsilon}, \mathbb{N}\right) \ge \bar{C}\varepsilon$,

otherwise a double choice for $\overline{N}_i$ is possible. Namely,

$$\overline{N}_i \in \left\{ \left\lfloor \frac{\alpha_{hex}\gamma}{L_i^\varepsilon} \right\rfloor - 1, \left\lfloor \frac{\alpha_{hex}\gamma}{L_i^\varepsilon} \right\rfloor \right\}, \quad \text{if} \quad \frac{\alpha_{hex}\gamma}{L_i^\varepsilon} - \left\lfloor \frac{\alpha_{hex}\gamma}{L_i^\varepsilon} \right\rfloor < \bar{C}\varepsilon;$$
$$\overline{N}_i \in \left\{ \left\lfloor \frac{\alpha_{hex}\gamma}{L_i^\varepsilon} \right\rfloor, \left\lfloor \frac{\alpha_{hex}\gamma}{L_i^\varepsilon} \right\rfloor + 1 \right\}, \quad \text{if} \quad \left\lfloor \frac{\alpha_{hex}\gamma}{L_i^\varepsilon} \right\rfloor + 1 - \frac{\alpha_{hex}\gamma}{L_i^\varepsilon} < \bar{C}\varepsilon.$$

This singularity affects the uniqueness of the limit velocity of each side. Indeed, if in the limit as $\varepsilon \to 0$, $\frac{\alpha_{hex}\gamma}{L_i} \notin \mathbb{N}$, then the velocity of the i-th side is uniquely determined by $\frac{\sqrt{3}}{2\gamma} \left\lfloor \frac{\alpha_{hex}\gamma}{L_i} \right\rfloor$. If, instead, $\frac{\alpha_{hex}\gamma}{L_i} \in \mathbb{N}$, then the velocity is not unique since it depends how the value $\frac{\alpha_{hex}\gamma}{L_i^\varepsilon}$ approaches $\mathbb{N}$ at the ε level. However, also in this case a limit velocity can be defined, leading to formulas (3.10).

The study of singular initial data, and the consequent *non-uniqueness* of limit evolutions, would require a more refined analysis (we refer to [17, Section 3.1.1] for a discussion). We just mention that if the initial datum is a regular Wulff-like hexagon with side length $L_0 = \alpha_{hex}\gamma$, then for every $T > 0$ and up to choosing properly the discrete motions E_k^ε, we can characterize the limit evolution as follows: for every $t \in [0, T]$, the initial hexagon stays pinned as in Theorem 3.6(a); then, for every $t > T$, it shrinks homothetically to its center as in Theorem 3.6(b).

Another feature we point out is the *partial* pinning of a side; that is, the side stays pinned until it becomes sufficiently short, due to the motion of the adjacent sides, and then moves. We enlighten this phenomenon through the following example, where we consider a particular class of symmetric convex Wulff-like hexagons.

Example (An example of partial pinning). We consider a symmetric initial set where a pair of sides stays pinned, at least for a finite time (see Fig. 13). Let $L_1^0 = L_4^0 =: L^{0,1} > \alpha_{hex}\gamma$, $L_6^0 = L_2^0 = L_3^0 = L_4^0 =: L^{0,2} < \alpha_{hex}\gamma$, with

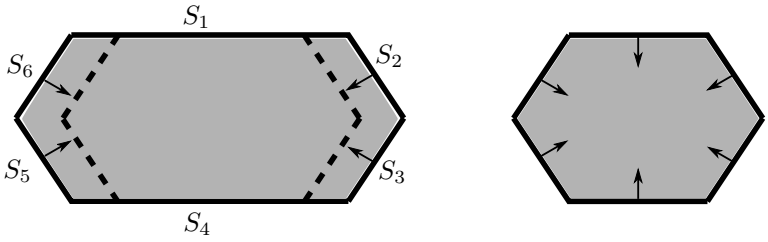

Figure 13. An example of partial pinning.

$L^{0,2} < L^{0,1}$ and $\frac{\alpha_{hex}\gamma}{L^{0,2}} \notin \mathbb{N}$. We examine the motion of sides S_1, S_2, S_3, since by symmetry the same holds for the triple S_4, S_5, S_6. We prove the following **Claim:** There exists $T > 0$ such that, for every $t \in [0, T]$, the side S_1 stays

pinned, $L_2(t) = L_3(t) \equiv L^{0,2}$ and the length $L_1(t)$ reduces with constant velocity according to

$$\dot{L}_1(t) = -\frac{2}{\gamma}\left\lfloor \frac{\alpha_{hex}\gamma}{L^{0,2}} \right\rfloor, \tag{3.21}$$

due to the motions of the neighboring sides S_2 and S_6.

Indeed, at every time t such that $v_1(t) = 0$, as a consequence of (3.5), (3.12), (3.13) and (3.11) we have $v_2(t) = v_3(t)$ and the laws for the side lengths of S_2 and S_3 are

$$\dot{L}_2(t) = \dot{L}_3(t) = 0,$$

with initial conditions $L_2(0) = L_3(0) = L^{0,2}$. This implies that $L_2(t) = L_3(t) = L^{0,2}$ and $v_2(t) = v_3(t) = \frac{\sqrt{3}}{2}\left\lfloor \frac{\alpha_{hex}\gamma}{L^{0,2}} \right\rfloor$. Thus, the effective motion consists of the translation, with constant velocity, of the pairs (S_2, S_3) and (S_5, S_6) in the directions $-\eta_1$ and η_1, respectively. The length of the side S_1 reduces according to the equation

$$\dot{L}_1(t) = -2\left(\frac{2}{\sqrt{3}\gamma} v_2(t)\right),$$

which corresponds to (3.21), and the same holds for S_4. Now, the time T is determined by $L_1(T) = \alpha_{hex}\gamma$ and this concludes the proof of Claim.

For $t > T$ the evolution is governed by equations

$$\dot{L}_1(t) = \frac{2}{\sqrt{3}}\left(v_1(t) - 2v_2(t)\right),$$

since $L_2(t) = L_6(t)$ for every t, where

$$\dot{L}_2(t) = -\frac{2}{\sqrt{3}} v_1(t),$$

and $v_1(t)$, $v_2(t)$ are as in (3.10).

3.4. A comparison with the crystalline motion with natural mobility

A natural question to address is to understand if the limit evolutions arising from the discrete version of the (ATW) scheme are comparable with the corresponding ones derived from its continuous counterpart. A first answer has been given by pinned sets, whose corresponding crystalline evolutions differ completely being nontrivial. On the contrary, the evolutions governed by (3.10)-(3.11) are not easily readable due to the complexity of the differential system, involving three side-lengths for each equation. Neverthless, according to Theorem 3.6(b), the evolution of each sufficiently small set homothetic to the Wulff set is governed by the single equation (3.20) until the extinction time (see Fig. 14). In this simple case, we can immediately compare (3.20) with the evolution law of the same initial sets by crystalline curvature with natural mobility that, as already remarked in the Introduction, can be defined independently of the (ATW) approach. In view of (1.5) and (3.2), the equation for $s(t)$ – the apothem of $E(t)$ – is given by

$$\dot{s}(t) = -\frac{8}{\sqrt{3}L(t)}.$$

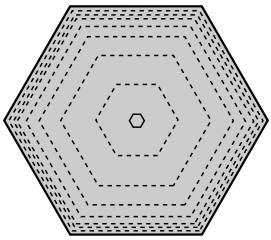

Figure 14. The evolution of a Wulff shape.

As a consequence, the corresponding law for the side length is

$$\dot{L}(t) = -\alpha_{hex}\frac{1}{L(t)},$$

showing that the limit evolution (3.20), when nontrivial, is slower than the corresponding crystalline evolutions. Moreover,

$$\lim_{\gamma\to+\infty} -\frac{1}{\gamma}\left\lfloor\frac{\alpha_{hex}\gamma}{L(t)}\right\rfloor = -\alpha_{hex}\frac{1}{L(t)}.$$

Acknowledgments. I would like to thank Marco Cicalese for suggesting this problem, Andrea Braides and Antonio Tribuzio for fruitful discussions.
I gratefully acknowledge the hospitality of the Technische Universität München, where a part of this work has been carried out, and the financial support of the TU Foundation Fellowship.

Appendix A.

A.1. The hexagonal norm

Let $\eta_1 := (1,0)$, $\eta_2 := (\frac{1}{2}, \frac{\sqrt{3}}{2})$ and $\eta_3 := \eta_1 - \eta_2$. For any $a > 0$ we define

$$\varphi_a(x) := a\sum_{k=1}^{3}|\langle x, \eta_k\rangle| \tag{A.1}$$

for every $x \in \mathbb{R}^2$. Recall that the norm φ_{hex} introduced in (2.5) coincides with $\varphi_{\frac{2}{3}}$.

We have the following simple result.

Lemma A.1. *Let φ_a be defined as in* (A.1). *Then φ_a is a norm on $\mathbb{R}^2$ and*

(i) $\{\varphi_a \le 1\} = \dfrac{1}{\sqrt{3}a}\mathrm{conv}(\pm\eta_1^\perp, \pm\eta_2^\perp, \pm\eta_3^\perp)$;

(ii) $\varphi_a^\circ(x) = \dfrac{1}{\sqrt{3}a}\max\limits_{k=1,2,3}|\langle x, \eta_k^\perp\rangle|$;

(iii) $\{\varphi_a^\circ \le 1\} = 2a\,\mathrm{conv}(\pm\eta_1, \pm\eta_2, \pm\eta_3)$.

Proof. Without loss of generality, we may assume that $a = 1$. In order to prove (i), we first note that $\varphi_1(\pm\eta_k^{\perp}) = \sqrt{3}$ for every $k = 1, 2, 3$. Now, if we denote by C_1 the set at the right hand side of (i) for $a = 1$, and take $x \in C_1$, then by convexity we deduce that $\varphi_1(x) \leq 1$. To conclude, we need to show that $\varphi_1(x) = 1$ for every $x \in \partial C_1$. In fact, since φ_1 is invariant under rotations with angle $\frac{\pi}{3}$, it will be sufficient to check the equality, e.g., on the boundary line segment defined by equations $x_1 = \frac{1}{2}$, $-\frac{1}{2\sqrt{3}} \leq x_2 \leq \frac{1}{2\sqrt{3}}$, and the assertion then follows by a straightforward computation. (ii) is an immediate consequence of the definition of dual norm

$$\varphi_1^{\circ}(\xi) := \max\{\langle \xi, x\rangle : \varphi_1(x) \leq 1\},$$

and of (i), since the linear function $\langle \xi, x\rangle$ on the compact convex polygon $\{\varphi_1(x) \leq 1\}$ attains its maximum at a vertex of the polygon (see, e.g., [33, Corollary 32.3.2]); the proof of (iii) is analogous to that of (i). □

A.2. Piecewise constant BV functions

We recall some basic properties of BV functions with values in a finite set we will need for the proof of Theorem 2.2 (see [1, Section 2.2] and the references therein).

Let Ω be a bounded open subset of $\mathbb{R}^n$. We denote by $SBV(\Omega; \{\pm 1\})$ the set of measurable functions $u : \Omega \to \{\pm 1\}$ whose distributional derivative Du is a measure with bounded total variation. Such a u can be written as

$$u = \sum_{k=1}^{\infty} \lambda_k \chi_{E_k}\,,$$

where $\lambda_k \in \{\pm 1\}$ and E_k are sets of finite perimeter. We denote by $S(u)$ the jump set of u and, for every $x \in S(u)$, $\nu_u(x)$ stands for the unit normal to $S(u)$ at x.

The following compactness and semicontinuity result holds (see, e.g., [1, Theorem 2.2]).

Theorem A.2. *Let $u_\varepsilon \in SBV(\Omega; \{\pm 1\})$ be such that*

$$\sup_{\varepsilon} \left(\int_{\Omega} |u_\varepsilon| \, \mathrm{d}x + \mathcal{H}^{n-1}(S(u_\varepsilon)) \right) < +\infty\,.$$

Then there exists a subsequence (not relabeled) and a function $u \in SBV(\Omega; \{\pm 1\})$ such that $u_\varepsilon \to u$ as $\varepsilon \to 0$ in $L^1(\Omega)$. Moreover, for any norm $\phi : \mathbb{R}^n \to [0, +\infty)$ it holds

$$\liminf_{\varepsilon \to 0} \int_{S(u_\varepsilon)} \phi(\nu_{u_\varepsilon})\, d\mathcal{H}^{n-1} \geq \int_{S(u)} \phi(\nu_u)\, d\mathcal{H}^{n-1}\,. \tag{A.2}$$

We introduce also some notation in order to apply a slicing technique (see, e.g., [4]). Let $n \geq 2$ and S^{n-1} be the unit sphere in $\mathbb{R}^n$. For $\xi \in S^{n-1}$, we denote by $\Pi^{\xi} := \{y \in \mathbb{R}^n : \langle y, \xi\rangle = 0\}$ the line through the origin orthogonal to ξ, and by $[y, y + \xi]$ the line segment with endpoints y and $y + \xi$. If $y \in \Pi^{\xi}$ and $A \subset \mathbb{R}^n$, we set $A^{\xi,y} := \{t \in \mathbb{R} : y + t\xi \in A\}$. Moreover, if $w : A \to \mathbb{R}$ we define its one-dimensional sections $w^{\xi,y} : A^{\xi,y} \to \mathbb{R}$ by $w^{\xi,y}(t) := w(y + t\xi)$.

The following characterization by slicing of an SBV function taking values in a finite set can be deduced, e.g., by [15, Theorem 2.6].

Theorem A.3. *Let $u \in SBV(\Omega;\{\pm 1\})$. Then, for all $\xi \in S^{n-1}$ the function $u^{\xi,y} \in SBV(\Omega^{\xi,y};\{\pm 1\})$ for $\mathcal{H}^{n-1}$-a.e. $y \in \Pi^\xi$. Moreover, we have*

$$\int_{\Pi^\xi} \#(S(u^{\xi,y}))\,\mathrm{d}\mathcal{H}^{n-1}(y) = \int_{S(u)} |\langle \nu_u, \xi\rangle|\,\mathrm{d}\mathcal{H}^{n-1}. \tag{A.3}$$

Conversely, if $u^{\xi,y} \in SBV(\Omega^{\xi,y};\{\pm 1\})$ for all $\xi \in \{\zeta_1, \zeta_2, \dots, \zeta_n\}$ basis of $\mathbb{R}^n$ and for $\mathcal{H}^{n-1}$-a.e. $y \in \Pi^\xi$, and

$$\int_{\Pi^\xi} \#(S(u^{\xi,y}))\,\mathrm{d}\mathcal{H}^{n-1}(y) < +\infty\,, \tag{A.4}$$

then $u \in SBV(\Omega;\{\pm 1\})$.

A.3. Proof of Theorem 2.2

The result of Theorem 2.2 will be an immediate consequence of Proposition A.4 below, once we note that for every E set of finite perimeter in Ω, the function $u := 2\chi_E - 1$ belongs to $SBV(\Omega;\{\pm 1\})$.

We introduce the class of piecewise constant functions

$$\mathcal{A}_\varepsilon(\Omega;\{\pm 1\}) := \left\{w : \mathbb{R}^2 \to \{\pm 1\} :\ w(x) = w(i) \text{ for all } x \in H_\varepsilon(i),\ i \in \varepsilon\mathbb{T}\right\},$$

where H_ε is the cell of the dual lattice of $\varepsilon\mathbb{T}$ as in Section 2.1, and define on $L^1(\Omega;\{\pm 1\})$ the energies

$$E_\varepsilon(w) := \begin{cases} \frac{1}{4} \displaystyle\sum_{\substack{(i,j)\in\varepsilon\mathbb{T}\times\varepsilon\mathbb{T}\\ |i-j|=\varepsilon}} \varepsilon(w(i)-w(j))^2\,, & \text{if } w \in \mathcal{A}_\varepsilon(\Omega;\{\pm 1\}) \\ +\infty\,, & \text{on } L^1(\Omega)\backslash\mathcal{A}_\varepsilon(\Omega;\{\pm 1\}). \end{cases} \tag{A.5}$$

We then have the following Γ-convergence result for these energies, which was mentioned in [1]. We provide here a proof by means of a slicing technique in the spirit of [15, Theorem 3.6] and following on the footsteps of [1, Theorem 4.1].

Proposition A.4. *Let $\varphi := \varphi_{\frac{2}{\sqrt{3}}}$ be defined as in* (A.1) *for $a = \frac{2}{\sqrt{3}}$. The energies E_ε defined as in* (A.5) *Γ-converge with respect to the L^1-topology to the functional*

$$E(u) = \begin{cases} \displaystyle\int_{S(u)} \varphi(\nu_u)\,\mathrm{d}\mathcal{H}^1\,, & \text{if } u \in SBV(\Omega;\{\pm 1\}), \\ +\infty\,, & \text{otherwise on } L^1(\Omega). \end{cases} \tag{A.6}$$

Proof. Let $u_\varepsilon \to u$ in $L^1(\Omega)$ be such that

$$\sup_\varepsilon E_\varepsilon(u_\varepsilon) < +\infty\,. \tag{A.7}$$

In order to prove the Γ-lim inf inequality for (A.6), we can split the energies E_ε by accounting separately for the contribution of pairs $(i,j) \in \varepsilon\mathbb{T} \times \varepsilon\mathbb{T}$

such that $i-j=\pm\xi\varepsilon$ for every $\xi\in\{\eta^1,\eta^2,\eta^3\}$. For this, we set

$$E_\varepsilon^\xi(u_\varepsilon):=\frac{1}{4}\sum_{i\in R_\varepsilon^\xi}\varepsilon(u_\varepsilon(i)-u_\varepsilon(i+\varepsilon\xi))^2 \tag{A.8}$$

where

$$R_\varepsilon^\xi:=\{i\in\varepsilon\mathbb{T}:\,[i,i+\varepsilon\xi]\subset\Omega\}\,,$$

so that we can write

$$E_\varepsilon(u_\varepsilon)=\sum_{\xi\in\{\eta^1,\eta^2,\eta^3\}}E_\varepsilon^\xi(u_\varepsilon)\,.$$

Then, it will be sufficient to prove that

$$\liminf_{\varepsilon\to0}E_\varepsilon^\xi(u_\varepsilon)\geq\frac{2}{\sqrt{3}}\int_{S(u)}|\langle\nu_u(x),\xi\rangle|\,\mathrm{d}\mathcal{H}^1(x)\,, \tag{A.9}$$

for every $\xi\in\{\eta^1,\eta^2,\eta^3\}$.

Let ξ be fixed. Setting

$$I_\varepsilon^\xi:=\{i\in R_\varepsilon^\xi:\,u_\varepsilon(i)\neq u_\varepsilon(i+\varepsilon\xi)\}\,,$$

from (A.8) we infer that

$$E_\varepsilon^\xi(u_\varepsilon)=\varepsilon\#(I_\varepsilon^\xi)\,. \tag{A.10}$$

Now, we note that Ω can be partitioned by the stripes $J_m^\xi\cap\Omega$ where

$$J_m^\xi:=\mathbb{R}\xi\times\left[\frac{\sqrt{3}}{2}m\varepsilon,\frac{\sqrt{3}}{2}(m+1)\varepsilon\right)\qquad m\in\mathbb{Z}\,.$$

Since $\#(I_\varepsilon^\xi\cap J_m^\xi)=\#(S(u_\varepsilon^{\xi,y}))$ for all $y\in J_m^\xi\cap\Pi^\xi$ and $m\in\mathbb{Z}$, (A.10) can be rewritten as

$$E_\varepsilon^\xi(u_\varepsilon)=\varepsilon\sum_{m\in\mathbb{Z}}\#(I_\varepsilon^\xi\cap J_m^\xi)=\frac{2}{\sqrt{3}}\int_{\Pi^\xi}\#(S(u_\varepsilon^{\xi,y}))\,\mathrm{d}\mathcal{H}^1(y)\,, \tag{A.11}$$

whence, passing to the liminf in both sides and by applying Fatou's lemma we obtain

$$\liminf_{\varepsilon\to0}E_\varepsilon^\xi(u_\varepsilon)\geq\frac{2}{\sqrt{3}}\int_{\Pi^\xi}\liminf_{\varepsilon\to0}\#(S(u_\varepsilon^{\xi,y}))\,\mathrm{d}\mathcal{H}^1(y)\,.$$

By virtue of the compactness part of Theorem A.2, for $n=1$, the assumption (A.7) together with the estimate (A.11) ensures that for $\mathcal{H}^1$-a.e. $y\in\Pi^\xi$ the sequence $u_\varepsilon^{\xi,y}$ is precompact in $SBV(\Omega^{\xi,y};\{\pm1\})$ and converges in L^1 to $u^{\xi,y}\in SBV(\Omega^{\xi,y};\{\pm1\})$. Thus, by (A.2) for $n=1$ we infer that

$$\liminf_{\varepsilon\to0}E_\varepsilon^\xi(u_\varepsilon)\geq\frac{2}{\sqrt{3}}\int_{\Pi^\xi}\#(S(u^{\xi,y}))\,\mathrm{d}\mathcal{H}^1(y)\,. \tag{A.12}$$

In view of (A.7), (A.12) implies that (A.4) holds true for every vector ξ of the basis $\{\eta_1,\eta_2\}$, whence $u\in SBV(\Omega;\{\pm1\})$ by virtue of Theorem A.3. To conclude, (A.9) follows by (A.12) and (A.3).

As for the upper bound, for any $u \in SBV(\Omega;\{\pm 1\})$ we have to construct a recovery sequence u_ε such that

$$\lim_{\varepsilon\to 0} E_\varepsilon(u_\varepsilon) = \int_{S(u)} \varphi(\nu_u)\,\mathrm{d}\mathcal{H}^1\,.$$

By density, it will suffice to consider u such that $S(u)$ is a polyhedral set. Up to a localization argument, we can further reduce to the case when $S(u)$ is an hyperplane; that is,

$$u(x) = \begin{cases} 1\,, & \text{if } \langle x,\nu\rangle \geq 0,\\ -1\,, & \text{otherwise,}\end{cases} \tag{A.13}$$

for a fixed vector ν. It is easy to see that, if $\nu \in \mathcal{R}$ is any coordinate direction of the lattice (see Section 2.1), the desired recovery sequence is provided by the discretization of the function (A.13) itself on the lattice. Namely, we define $u_\varepsilon \in \mathcal{A}_\varepsilon(\Omega;\{\pm 1\})$ as $u_\varepsilon(i) := u(i)$ for any $i \in \varepsilon\mathbb{T}\cap\Omega$.

The argument can be extended to the case when $S(u)$ is a finite connected union of line segments with normal belonging to $\mathcal{R}$, and then for $S(u)$ consisting of a line with normal $\nu \notin \mathcal{R}$ (cf. the constructions for the proof of [15, Proposition 5.2 and 5.3]). □

References

[1] R. Alicandro, A. Braides and M. Cicalese, Phase and anti-phase boundaries in binary discrete systems: a variational viewpoint. *Netw. Heterog. Media* **1** (2006), 85–107.

[2] F. Almgren and J.E. Taylor, Flat flow is motion by crystalline curvature for curves with crystalline energies. *J. Diff. Geom.* **42** 1 (1995), 1–22.

[3] F. Almgren, J.E. Taylor and L. Wang, Curvature driven flows: a variational approach. *SIAM J. Control Optim.* **50** (1993), 387–438.

[4] L. Ambrosio, N. Fusco, and D. Pallara, *Functions of bounded variation and free discontinuity problems*, Oxford Mathematical Monographs, Clarendon Press, Oxford (2000).

[5] S. Angenent and M.E. Gurtin, Multiphase thermodynamics with interfacial structure 2. Evolution of an isothermal interface. *Arch. Rational Mech. Anal.* **108** (1989), 323–391.

[6] Y. Au Yeung, G. Friesecke and B. Schmidt, Minimizing atomic configurations of short range pair potentials in two dimensions: crystallization in the Wulff shape. *Calc. Var. PDE* **44** (2012), 81–100.

[7] A. Bach, M. Cicalese, L. Kreutz and G. Orlando, The antiferromagnetic XY model on the triangular lattice: chirality transitions at the surface scaling (2020), Preprint `https://arxiv.org/abs/2004.01416`.

[8] K. Bhattacharya and B. Craciun, Effective motion of a curvature-sensitive interface through a heterogeneous medium. *Interfaces Free Bound.* **6** (2004), 151–173.

[9] G. M. Bell and D. A. Lavis, Two-dimensional bonded lattice fluids. I. Interstitial model, *J. Phys. A* **3**, 427 (1970).

[10] G. M. Bell and D. A. Lavis, Two-dimensional bonded lattice fluids. II. Orientable molecule model, *J. Phys. A* **3**, 568 (1970).

[11] A. Braides, *Approximation of Free-Discontinuity Problems*, Lecture Notes in Mathematics **1694**, Springer Verlag, Berlin, 1998.

[12] A. Braides. Γ-*convergence for Beginners*. Oxford University Press, Oxford, 2002.

[13] A. Braides, M. Cicalese and N. K. Yip, Crystalline Motion of Interfaces between Patterns. *J. Stat. Phys.* **165**(2) (2016), 274–319.

[14] A. Braides, *Local Minimization, Variational Evolution and* Γ-*convergence*. Lecture Notes in Mathematics, 2094, Springer Verlag, Berlin, 2014.

[15] A. Braides and M. S. Gelli, Analytical treatment for the asymptotic analysis of microscopic impenetrability constraints for atomistic systems. *ESAIM: M2AN* **51** (2017), 1903–1929.

[16] A. Braides and M. S. Gelli, Asymptotic analysis of microscopic impenetrability constraints for atomistic systems. *J. Mech. Phys. Solids* **96** (2016), 235–251.

[17] A. Braides, M.S. Gelli and M. Novaga, Motion and pinning of discrete interfaces. *Arch. Ration. Mech. Anal.* **195** (2010), 469–498.

[18] A. Braides, A. Malusa and M. Novaga, Crystalline evolutions with rapidly oscillating forcing terms. *Ann. Sc. Norm. Super. Pisa Cl. Sci.* (5) Vol. XX (2020), 143–175.

[19] A. Braides and A. Piatnitski, Homogenization of surface and length energies for spin systems, *J. Funct. Anal.* **264** (2013), 1296–1328.

[20] A. Braides and G. Scilla, Motion of discrete interfaces in periodic media. *Interfaces Free Bound.* **15** (2013), 451–476.

[21] A. Braides and G. Scilla, Nucleation and backward motion of discrete interfaces. *C. R. Acad. Sci. Paris* **351** (21-22) (2013), 803–806.

[22] A. Braides, G. Scilla and A. Tribuzio, Nucleation and backward motion of anysotropic discrete interfaces. *In progress* (2020).

[23] A. Braides and M. Solci, Motion of discrete interfaces through mushy layers. *J. Nonlinear Sci.* **26** (2016), 1031–1053.

[24] A. Braides, M. Solci and E. Vitali, A derivation of linear elastic energies from pair-interaction atomistic systems, *Netw, Heterog. Media*, **2** (2007), 551–567.

[25] V. Caselles and A. Chambolle, Anisotropic curvature-driven flow of convex sets. *Nonlinear Anal.* **65** (8) (2006), 1547–1577.

[26] A. Chambolle, An algorithm for mean curvature motion. *Interfaces Free Bound.* **6** (2) (2004), 195–218.

[27] A. Chambolle and M. Novaga, Convergence of an algorithm for the Anisotropic and Crystalline Mean Curvature Flow, *SIAM J. Math. Anal.* **37** (6), 1978–1987.

[28] E. Davoli, P. Piovano and U. Stefanelli, Sharp $N^{3/4}$ Law for the Minimizers of the Edge-Isoperimetric Problem on the Triangular Lattice. *J Nonlinear Sci* **27** (2017), 627–660.

[29] L. De Luca, Γ-convergence analysis for discrete topological singularities: the anisotropic triangular lattice and the long range interaction energy. *Asymptot. Anal.* **96** (2016), 185–221.

[30] N. Dirr and N. K. Yip, Pinning and de-pinning phenomena in front propagation in heterogeneous media. *Interfaces Free Bound.* **8** (2006), 79–109.

[31] A. Malusa and M. Novaga, Crystalline evolutions in chessboard-like microstructures. *Netw. Heterog. Media* **13** (3) (2018), 493–513.

[32] F. Morgan, *Riemannian geometry: a beginner's guide.* Jones and Bartlett Publisher, Boston, (1993).

[33] R. Rockafellar, *Convex Analysis.* Princeton University Press, (1970).

[34] M. Ruf, Motion of discrete interfaces in low-contrast random environments. *ESAIM: COCV* **24** (3) (2018), 1275–1301.

[35] G. Scilla, Motion of discrete interfaces in low-contrast periodic media. *Netw. Heterog. Media* **9** (2014), 169–189.

[36] J. E. Taylor, A Variational Approach to Crystalline Triple-Junction Motion. *J. of Stat. Phys.* **95** (1999), 1221–1244.

[37] J.E. Taylor, Motion of curves by crystalline curvature, including triple junctions and boundary points, *Differential Geometry, Proceedings of Symposia in Pure Math.* **51** (part 1) (1993), 417–438.

[38] J.E. Taylor, Some mathematical challenges in materials science. *Bull. Amer. Math. Soc.* **40** (1) (2003), 69–87.

[39] J.E. Taylor, J. Cahn and C. Handwerker, Geometric Models of Crystal Growth. *Acta Metall. Mater.* **40** (1992), 1443–1474.

[40] J.E. Taylor, J. Cahn and C. Handwerker, Mean Curvature and Weighted Mean Curvature. *Acta Metall. Mater.* **40** (1992), 1475–1485.

[41] F. Theil, A proof of crystallization in two dimensions. *Comm. Math. Phys.* **262** (2006), 209–236.

Giovanni Scilla
Department of Mathematics and Applications "R. Caccioppoli"
University of Naples "Federico II"
Via Cintia, Monte S. Angelo - 80126 Naples
(ITALY)
e-mail: giovanni.scilla@unina.it